Final Report for

Advanced Techniques for High-Performance Computer Simulations of Rarefied Neutral Gas and Plasma Flows

NASA Grant NNG04GQ73G from a proposal to
the Applied Information Systems Research Program

for the period October 1, 2004 to December 31, 2005

Principal Investigator

Michael R. Combi
Department of Atmospheric, Oceanic and Space Sciences
University of Michigan
Space Research Building
2455 Hayward Street
Ann Arbor, MI 48109
Tel: 1 (734) 764-7226
Fax: 1 (734) 647-3083
Email: mcombi@umich.edu

1. Introduction

In order to understand the global structure, dynamics, and physical and chemical processes occurring in the upper atmospheres, exospheres, and ionospheres of the Earth, the other planets, comets and planetary satellites and their interactions with their outer particles and fields environs, it is often necessary to address the fundamentally non-equilibrium aspects of the physical environment. These are regions where complex chemistry, energetics, and electromagnetic field influences are important. Traditional approaches are based largely on hydrodynamic or magnetohydrodynamic (MHD) formulations and are very important and highly useful. However, these methods often have limitations in rarefied physical regimes where the molecular collision rates and ion gyrofrequencies are small and where interactions with ionospheres and upper neutral atmospheres are important.

At the University of Michigan we have an established base of experience and expertise in numerical simulations based on particle codes that address these physical regimes. The Principal Investigator, Dr. Michael Combi, has over 20 years of experience in the development of particle-kinetic and hybrid kinetic/hydrodynamics models and their direct use in data analysis. He has also worked in ground-based and space-based remote observational work and on spacecraft instrument teams. His research has involved studies of cometary atmospheres and ionospheres and their interaction with the solar wind, the neutral gas clouds escaping from Jupiter's moon Io, the interaction of the atmospheres/ionospheres of Io and Europa with Jupiter's corotating magnetosphere, as well as Earth's ionosphere.

Grants from the Applied Information Systems Research Program (AISRP) have supported the basic construction and first applications of three-dimensional, neutral and ion kinetic particle models, which have potential application to various space science problems. The purpose of this grant, which resulted from a selection for one year of funding at reduced support, was to continue some unfinished work, including publication of ongoing work, and to bridge to a new proposed work. The new proposal was declined. The main new task was in the area of exploring the possibility to integrate kinetic and hydrodynamic methodologies into one code for application to space science applications. This report describes our progress during this year.

2. A Kinetic Hybrid Particle Code for Application to Space Science

This year saw the publication of our paper (*Lipatov and Combi*, 2006) begun with previous support from the AISRP to perform kinetic hybrid particle calculations for applications to space science. The application was for the interaction of Jupiter corotating magnetized plasma with the volcanically produced atmosphere of its moon Io. A copy of this paper is attached to this report.

3. Hybrid DSMC/CFD Approach

Simulations of real gas flow often require numerical solutions with a wide variation of macroscopic parameters in the computational domain. In some cases, the gas flow in a part of the domain could be in a rarefied regime while another part may be in continuum regime. Rarefied flow conditions appear in different kinds of circumstances in the numerical study of cometary comae (e.g., the Knudsen layer at the surface, on the night side of nuclei, at large distances from the nucleus and for weak comets in general). Even though the kinetic approach is generally appropriate physically to study gas flows even in the fluid limit (because the fluid equations themselves are approximations of the general kinetic formulation), it might make the numerical simulations of the flow less efficient computationally. So, developing an efficient numerical approach that can be used for simulation of gas systems under continuum/rarefied conditions is

an important problem of modern numerical gas dynamics. An approach that utilizes DSMC and fluid (CFD) methodologies in different subdomains has been described in various papers [*Bird*, 1998; *Ivanov et al.*, 2000; *Ivanov and Markelov*, 2000; *Hash and Hassan*, 1996; *Roy et al.*, 2002; *Wang and Boyd*, 2003; *Wang et al.*, 2002].

We were successful in building and testing the hybrid Euler/DSMC code, but we found two main negative results in applying the technique to comets. The first one questions the utility of the practical speed-up of the method when applied to the intended application, comets. The second potentially indicates that an Euler solver may never actually be adequately applied to the comet problem. Both are actually important negative results in indicating the appropriate direction for future practical methodologies for these transitional space science applications.

The first is that while the Euler (CFD) solver is of course faster computationally than a DSMC calculation on a cell-by-cell basis, even when the DSMC is applied with collision limiting in the collisional limit, practical savings to computation time were not realized. Unless the computational volume is dominated by a significant fraction of computational cells that can be treated with the Euler solver, the savings is small. In the dusty-gas cometary application for which were developing this technique, most of the volume, and therefore most of the cells, still need to be treated in the kinetic limit. For example if 10% of the cells can be computed with the Euler solver and there is a speed-up, even of a factor of ten, the resulting computational savings is only 9%. In reality, there is significant complication added to treat the boundary layers between the two domains. In the comet case there is a kinetic domain within a few meters of the surface and then a fluid domain extending from a few meters to typically hundreds of kilometers and then another kinetic domain extending to a million km an more. Even though the number of cells is kept reasonable because their sizes increase geometrically with distance from the nucleus, there is still a complicated boundary between the domains where accurate macroparameters need to be collected from the kinetic simulation for specifying the Euler conditions, and conversely new particle creation needs to be specified for entrance into the kinetic regime from the Euler volumes.

The second issue deals with the interface between the kinetic and fluid domains for the comet application in particular. It appears that even for the simplest 1D spherical flow model, wherever the boundary is placed between the fluid and DSMC regimes, the variation of the macroparameters is always continuous in value but their derivatives (or slopes) are sometimes not. The problem is worst for the most difficult macroparameter, the temperature, which is based on the second moment of the distribution function. Moving the boundary well into the fluid regime helps but does not eliminate the problem, and further complicates the first issue by decreasing the size of the fluid domain. The results are demonstrated in Figures 1 - 4.

4. Two-Phase (Dust and Gas) Kinetic Model with Sublimating Grains

The cometary literature has been filled with suggestions that icy grains may be released with dust from the nucleus of the comet, dragged away with the gas flow, and contribute to an "extended" source of gas that might have significant impact on the physical state of the entire atmosphere (*Huebner and Weigert* 1966; *Delsemme and Wenger* 1970; *Delsemme and Miller* 1971). The bright comet Hyakutake (C/1996 B2) raised further direct evidence for the existence of icy grains and large icy fragments clearly producing a significant fraction of additional gas away from the nucleus. There has been little or no physical modeling of the potential dynamical and thermodynamical effects of the inclusion of such extended sources on the coma.

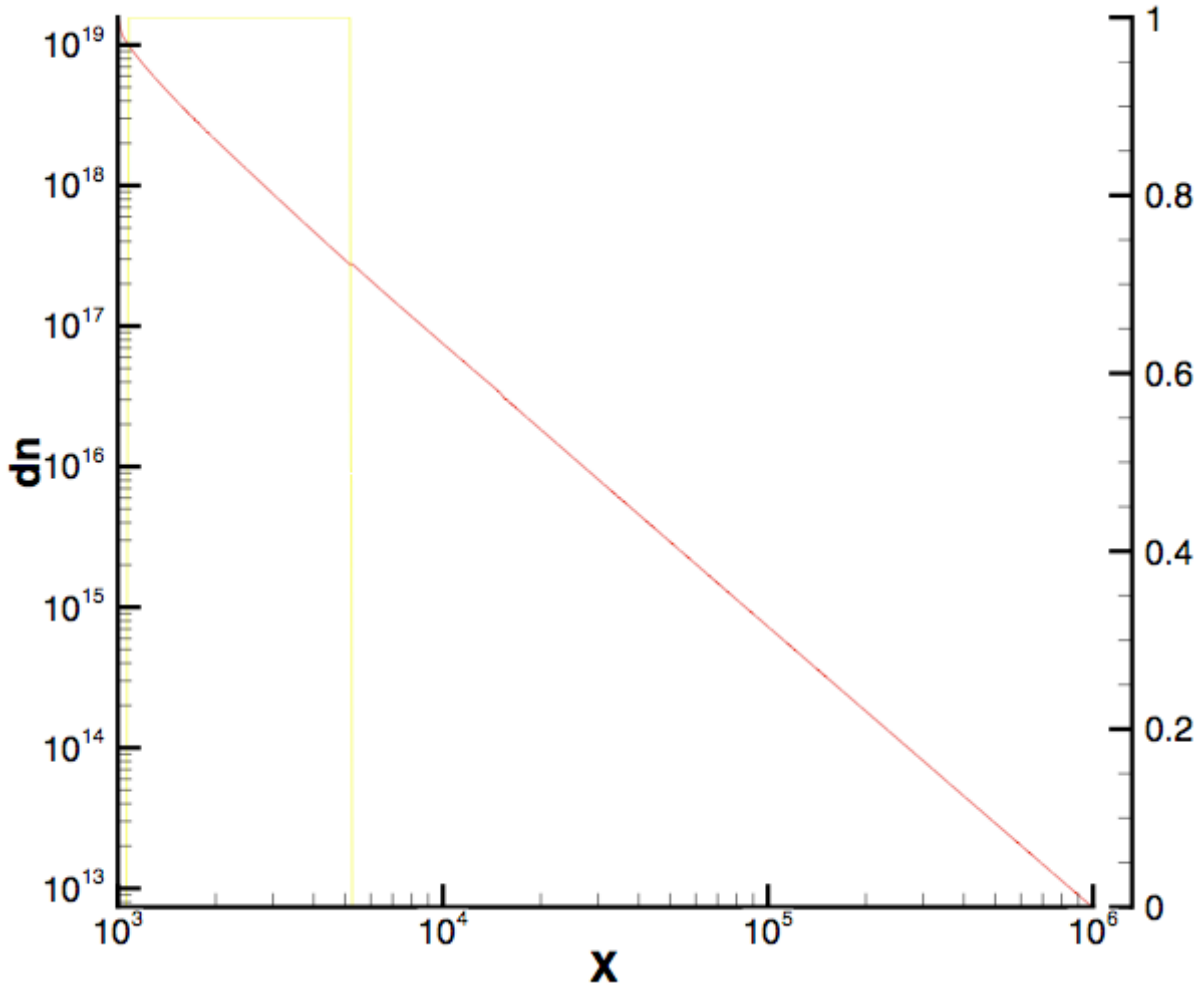

Figure 1. **Gas Density in a Cometary Coma with a Hybrid Euler/DSMC Model.** The red line shows the gas density (meters^{-3}) in the coma as a function of distance from the center of the nucleus of the comet (meters). The yellow box indicates the volume computed with the Euler solver. The small region to the left of the yellow box is the Knudsen layer at the surface and the expansion region region to the right of the yellow box are both computed using the kinetic DSMC model. The small discontinuity in the slope of the line is more apparent on the right edge of the yellow box, but is also present on the left.

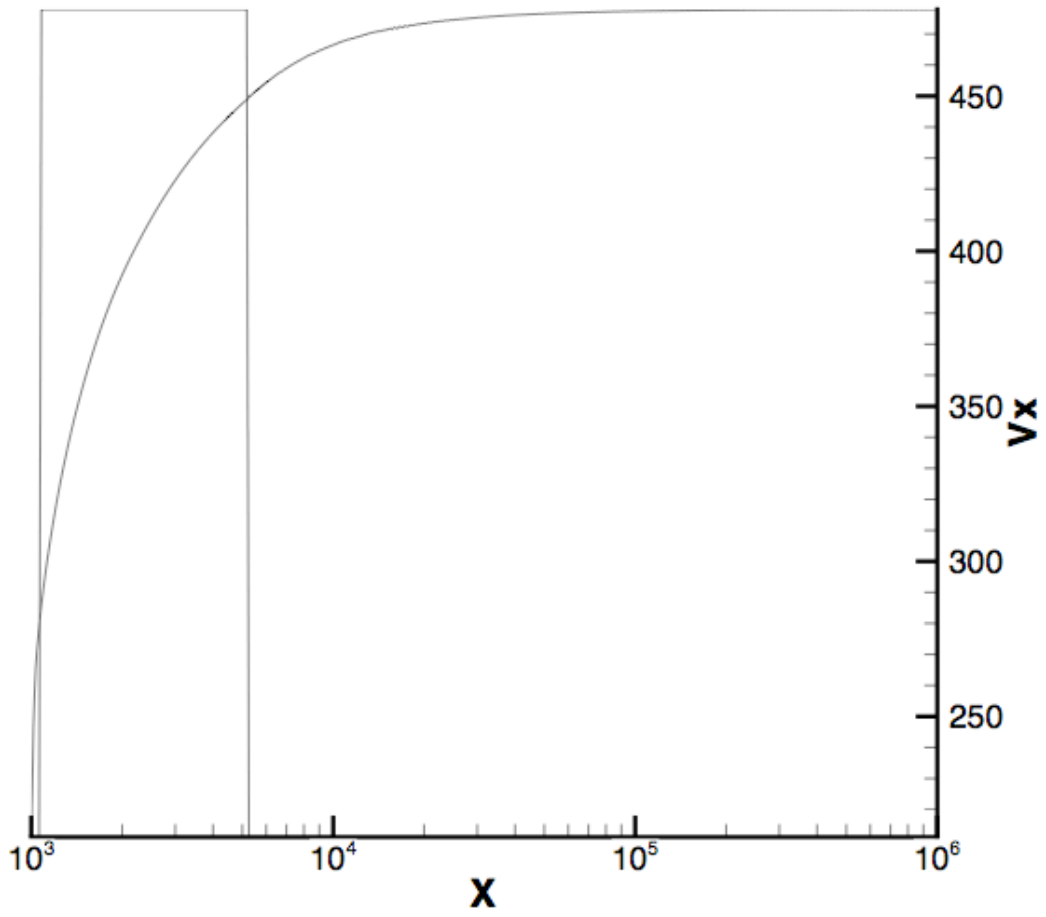

Figure 2. **Gas Velocity in a Cometary Coma with a Hybrid Euler/DSMC Model.** The box to the left corresponds to the yellow box in Figure 1. Here the curved line gives the gas velocity in meters s^{-1} as a function of distance from the center of the nucleus (in meters). The discontinuity in the slope of the velocity at the boundaries between the Euler and DSMC regimes is not as bad as either the density or the temperature.

The early informal reporting of "arcs" of gas in the distribution of the minor carbon radicals in images of Hyakutake raised some interesting possibilities. The discovery that the arcs were present in the distribution of OH, the main by-product of water the most abundant gas species in comets, meant that the arcs were a fundamental feature of the comets tenuous atmosphere (or coma) itself. *Harris et al.* (1997) reported the existence of CN and OH gas arcs in comet Hyakutake, and we performed DSMC modeling of the arcs as part of that discovery paper as an interaction of two sources of gas, one from the nucleus and one from the released fragments which were seen moving slowly down the tail of the comet. In addition to the individual large fragments there was significant independent evidence for multiple outbursts by the comet where many small particles were released, raising the gas production rate of the whole atmosphere by a

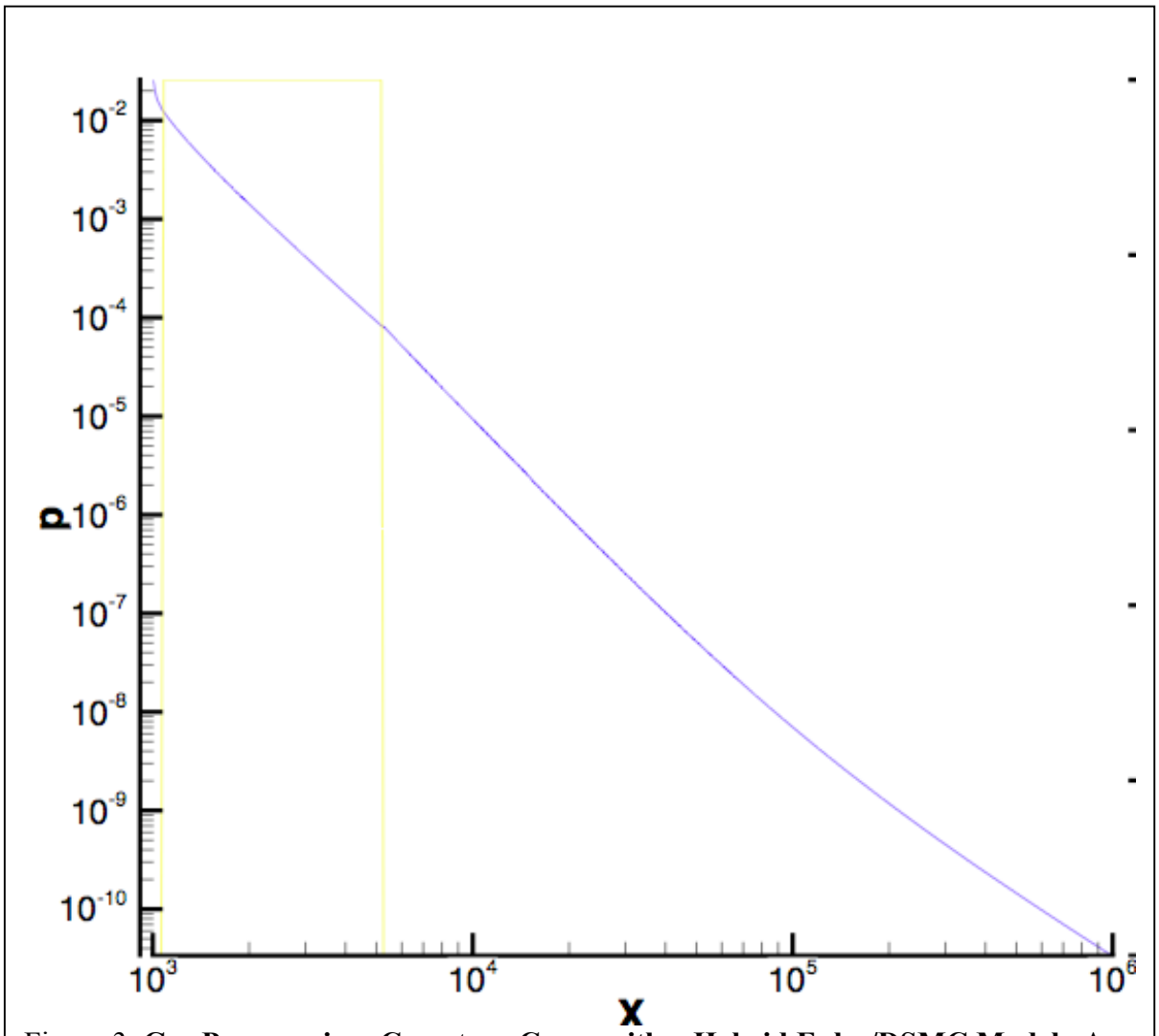

Figure 3. **Gas Pressure in a Cometary Coma with a Hybrid Euler/DSMC Model.** As in Figures 1 and 2 the yellow box to the left again separates the inner Knudsen layer to the left of the box, the fluid region inside the box and the outer expansion region to the right of the box. Here the changes in slope are again apparent.

factor of 3. This meant that for times of a few days, the ejected cloud of particles produced more gas than originally vaporized from the nucleus.

We have modified our dusty-gas DSMC model to include the effects of sublimating grains on the dynamics of the coma. This required some fundamental changes to the source/ boundary parts of the code. Grains of a specified size distribution and water content are released just like the dust particles from the surface of the nucleus, but are then allow to sublimate as they are heated by sunlight. They are fully coupled collisionally to the gas. We have completed the inclusion and testing of this feature in our parallelized DSMC model as part of the this project and are now completing runs and analysis of observations of dust and gas in comet Hyakutake as part of one of our planetary research and analysis grants. The results are being incorporated as part of the doctoral dissertation of Mr. Valeriy Tenishev and will be written into a paper to be published in an archival journal -- Icarus or Astrophysical Journal -- later this year. Preliminary versions of these results were presented at the 2005 Division for Planetary Sciences meeting in

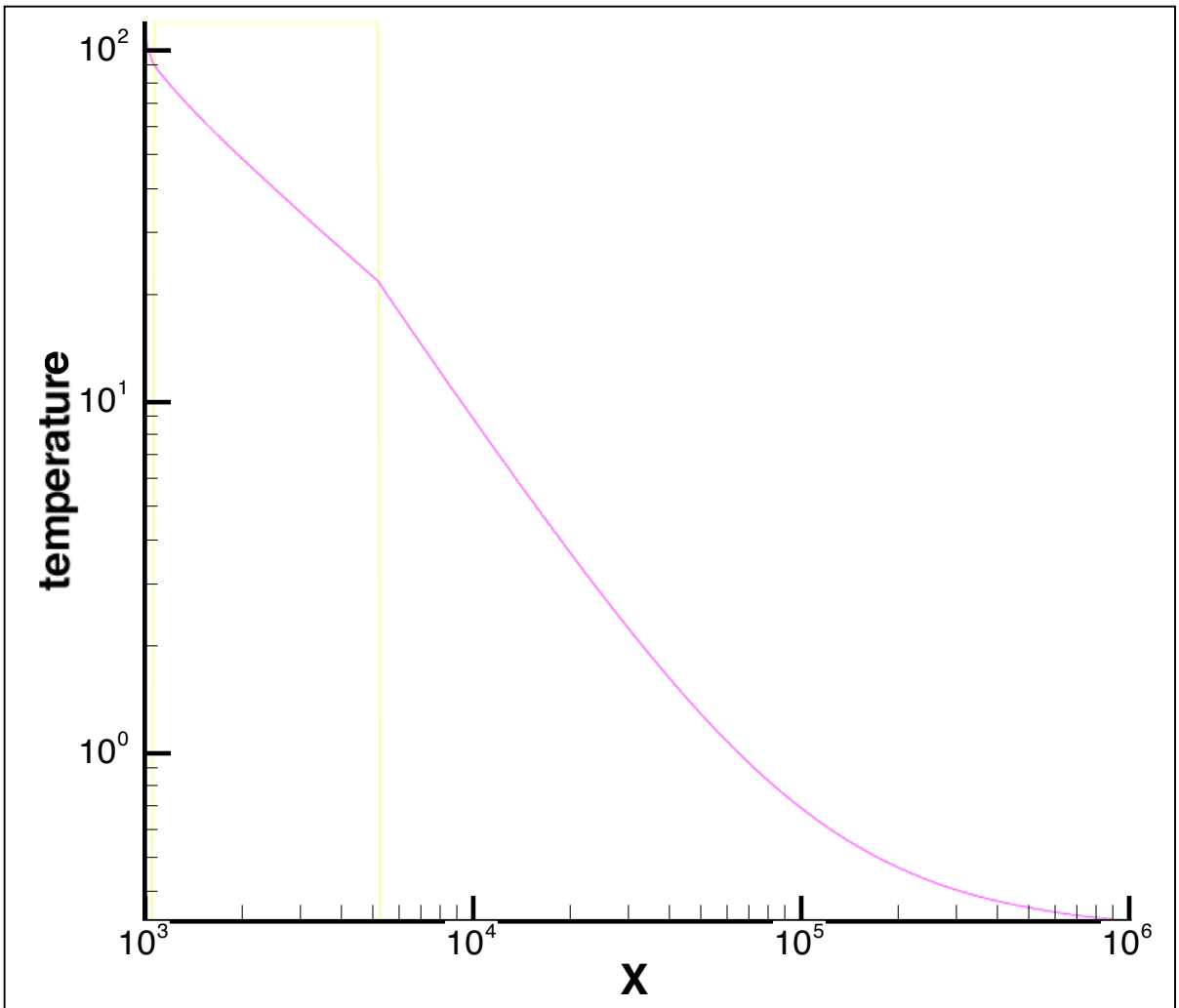

Figure 4. **Gas Temperature in a Cometary Coma with a Hybrid Euler/DSMC Model.** As in Figures 1 - 3 the yellow box to the left again separates the inner Knudsen layer to the left of the box, the fluid region inside the box and the outer expansion region to the right of the box. Here the changes in slope are again apparent.

Cambridge, England (*Combi and Tenishev*, 2005) and the Fall AGU meeting (*Combi and Tenishev,* 2005) as work progressed.

Figure 5 shows plots of the gas velocity and temperature as a function of distance from the center of the nucleus for comet Hyakutake as modeled with our dusty-gas DSMC code with sublimating grains. The solid lines give the pure gas model as a baseline and the dashed line gives a model with the same level of gas production from the nucleus but with an additional factor of 2 gas production from outflowing sublimating icy grains.

As part of continuing research and analysis grants from NASA we are now using the code and adjusting the various parameters, such as the particle size distribution and the size of the icy grain outburst, in order to have the model compare favorably with observations of gas and dust outflow during one of the comet's outbursts (*Samarasinha et al.*, 2004).

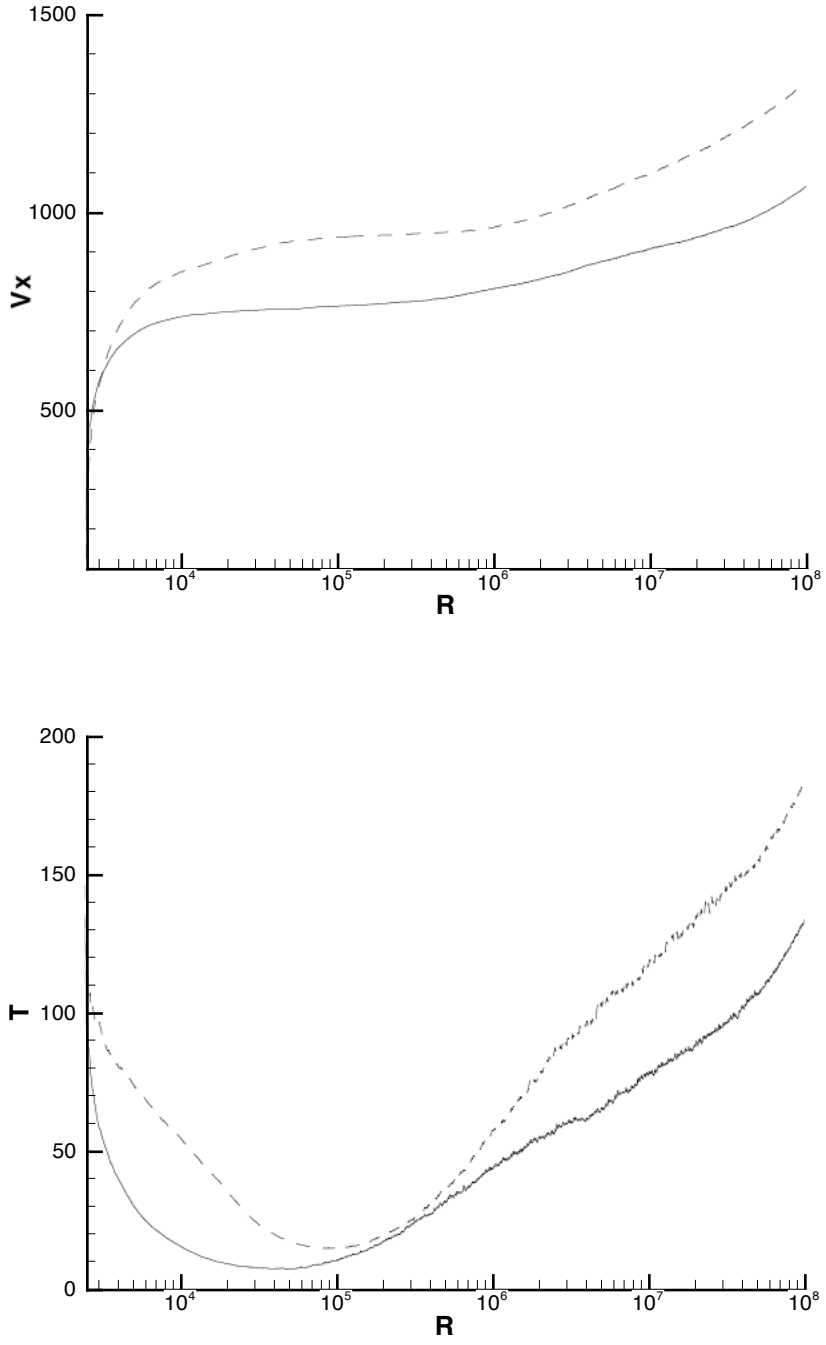

Figure 5. **Gas Flow in comet Hyaktutake with Sublimating Grains.** Above is a plot of the gas velocity and below the gas temperature for comet Hyakutake both as functions of distance (R) from the center of the nucleus in meters. The velocity is in meters s^{-1}, the temperature is in Kelvins. The solid line is the pure gas model for comparison. The dashed line includes the sublimating grains.

5. Kinetic Dusty-Gas Modeling Support for the Rosetta Mission.

One of the important goals of the AISRP is to provide new computational tools for use in future NASA programs. An interdisciplinary international modeling effort is underway, organized by the International Space Science Institute (ISSI) in Bern, Switzerland, in association with the Rosetta project (ESTEC) and the JPL Rosetta project (the support and organizing infrastructure for US investigators on the Rosetta project). As part of this effort, this PI is the lead investigator in the area of dusty-gas coma modeling (with T. Gombosi, U. Michigan and N. Thomas, U. Bern). The larger effort involves several other teams of investigators performing (1) MHD modeling of the comet/solar-wind interaction (T. Gombosi, K. Hansen, and M. Combi, U Michigan), (2) nucleus and surface-boundary modeling (B. Davidsson and H. Rickman, Uppsala U.), (3) electron energetics (T. Cravens U. Kansas), (4) plasma hybrid modeling (U. Motschmann and T. Bagdonat, MPI Braunschweig), (5) coma chemistry (K. Altwegg, U. Bern, and the entire U. Michigan group). Rosetta Project Scientist G. Schwehm and US Rosetta Project (JPL) Scientist C. Alexander are also participants, as are a number of other Rosetta scientists. We have been performing dusty-gas DSMC model calculations using our code developed as part of grants from the AISR program -- this one as well as previous ones. The work is also supported in concert with other NASA grants from Headquarters and through JPL.

A first set of coupled results was presented at the 2005 Division for Planetary Sciences meeting (*Hansen et al.* 2005). The dusty-gas DSMC results are shown in Figure 6. A preliminary version of the DSMC results alone had been presented at the 2004 DPS meeting along with a description of the nucleus thermophysical model by our collaborator Bjorn Davidsson (Uppsala University) that produces the atmospheric dusty-gas source from the nucleus (*Tenishev, Combi and Davidsson*, 2004). The quantitative neutral coma results are then use for input into MHD and hybrid kinetic models for the comet/solar-wind interaction.

A complete set of publications and presentations with citable references during the funding period resulting from AISRP funding is given at the end of this report.

References

Bird, G.A., Recent Advances and Current Challenges for DSMC, *Computers Math. Applic. Vol. 35, No. 1,* 1998.

Combi, M.R. and V.M. Tenishev. Modeling the Coma Dynamics of a Comet with an Icy Grain Halo. American Geophysical Union, Fall Meeting 2005, abstract #P11A-0101, 2005.

Combi, M.R. and V.M. Tenishev. The Effects of Extended Sources of Gas on Cometary Coma Dynamics. American Astronomical Society, DPS meeting #37, #16.04, 2005.

Delsemme, A.H. and D.C. Miller. Physico-chemical phenomena in comets -III The Continuum of comet Burnham (1960 II). Planet. Space Sci. 19, 1229-1257, 1971.

Delsemme, A.H. and A. Wenger. 1970. Physico-chemical phenomena in comets-I. Experimental Study of Snows in a Cometary Environment. Planetary & Space Sci. 18, 709-715.

Desvoivres, E., J. Klinger, A.C. Levasseur-Regourd, and G.H. Jones. 2000. Modeling the dynamics of cometary fragments: Application to comet C/1996 B2 Hyakutake. Icarus 144, 172-181.

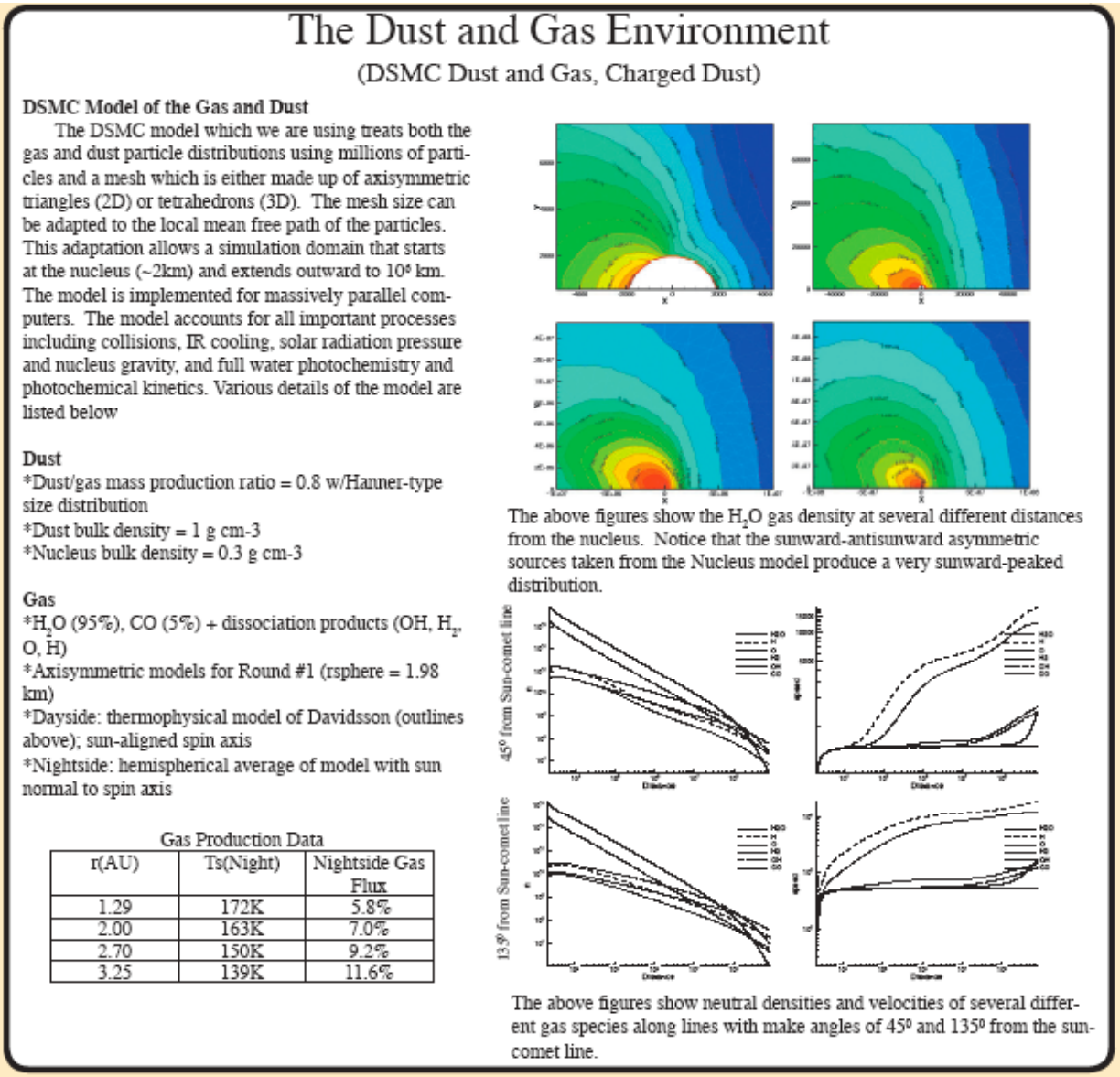

Figure 6. Dusty-Gas DSMC Model Results for Comet 67P/Churyumov-Gerasimenko throughout the Rosetta Mission. Above are the dusty-gas results presented at the 2005 Division for Planetary Sciences meeting using our dusty-gas DSMC comet model. The calculations are used to predict the dusty-gas environment around the nucleus and to serve as the source for ions as quantitative input into MHD and hybrid plasma models for the interaction of the comet with the solar wind.

Hansen, K. C., Alexander, C. J., Altwegg, K., Bagdonat, T., Bertini, I., Coates, A. J., Combi, M. R., Cravens, T. E., Davidsson, B. J. R., Geiss, J., and 9 coauthors. Rosetta-ISSI Comet 67P/Churyumov-Gerasimenko Environment Model. American Astronomical Society, DPS meeting #37, #16.08, 2005.

Hash, D.B., H.A. Hassan, Assessment of Schemesfor Coupling Monte Carlo and Navier-Stokes Solution Method, *J. Thermophysics and Heat Transfer, Vol. 10, No. 2,* 1996.

Harris, W.M., M.R. Combi, R.K. Honeycutt, and B.E.A. Mueller. 1997. Evidence for interacting gas flows and an extended volatile source distribution in the coma of comet C/1996 B2 (Hyakutake). Science 277, 676-681.

Huebner, W.F. and A. Weigert. Eiskörner in der Koma von Kometen. Z. für Astrophy. 64, 185-201, 1966.

Ivanov, M., G. Markelov, *Numerical Study of Thruster Nozzle Plume, AIAA 2000-0468*, 2000

Ivanov, M.S., G.N. Markelov, Ye.A. Bondar, Numerical Simulation of Thruster Plumes in Cryogenic Vacuum Facility, *AIAA 2000-2502*, 2000.

Roy C. J., M. A. Gallis, T. J. Bartel, J. L. Payne, Navier-Stokes and DSMC Simulations for Hypersonic Laminar Shock-Shock Interaction Flows, *AIAA 2002-0737*, 2002.

Samarasinha, N.H., D.G. Schleicher, L.M. Woodney. Modeling CN Jets of Comet Hyakutake (C/1996 B2). American Astronomical Society, DPS meeting #36, #33.13, 2004.

Tenishev, V., Combi, M., Davidsson. Kinetic dusty-gas coma models for comet 67P/Churyumov-Gerasimenko. B. AAS/Division for Planetary Sciences Meeting Abstracts #36, #33.16, 2004.

Wang, W.-L., I. D. Boyd, Continuum Breakdown in Hypersonic Viscous Flows, *AIAA 2002-0651,* 2002.

Wang, W.-L., Q. Sun and I. D. Boyd, Towards Development of a Hybrid DSMCCFD Method for Simulating Hypersonic Interacting Flows, *AIAA 2002–3099*, 2002.

Publications/Presentations Supported by the AISRP during the Reporting Period

• Lipatov, A.S. and M.R. Combi. Effects of Kinetic Processes in Shaping Io's Global Plasma Environment: A 3D Hybrid Model. *Icarus* **180**, 412-427 2006.

• Combi, M.R. and V.M. Tenishev. Modeling the Coma Dynamics of a Comet with an Icy Grain Halo. American Geophysical Union, Fall Meeting 2005, abstract #P11A-0101, 2005.

• Combi, M.R. and V.M. Tenishev. The Effects of Extended Sources of Gas on Cometary Coma Dynamics. American Astronomical Society, DPS meeting #37, #16.04, 2005.

• Hansen, K. C., Alexander, C. J., Altwegg, K., Bagdonat, T., Bertini, I., Coates, A. J., Combi, M. R., Cravens, T. E., Davidsson, B. J. R., Geiss, J., and 9 coauthors. Rosetta-ISSI Comet 67P/Churyumov-Gerasimenko Environment Model. American Astronomical Society, DPS meeting #37, #16.08, 2005.

• Tenishev, V., Combi, M., Davidsson. Kinetic dusty-gas coma models for comet 67P/Churyumov-Gerasimenko. B. AAS/Division for Planetary Sciences Meeting Abstracts #36, #33.16, 2004.

Available online at www.sciencedirect.com
SCIENCE DIRECT
Icarus 180 (2006) 412–427
ICARUS
www.elsevier.com/locate/icarus

Effects of kinetic processes in shaping Io's global plasma environment: A 3D hybrid model

Alexander S. Lipatov [a,b,c,*], Michael R. Combi [a]

[a] *Space Physics Research Laboratory, Department of Atmospheric, Oceanic and Space Sciences, The University of Michigan, Ann Arbor, MI 48109-2143, USA*
[b] *Dialogue-Science, A.A. Dorodnitsyn Computing Center Russian Academy of Sciences, Vavilova St. 40, 119991 Moscow, Russia*
[c] *Department of Problems of Physics and Energetics, Moscow Institute of Physics and Technology, Moscow Reg., Russia*

Received 18 November 2004; revised 12 August 2005

Available online 11 November 2005

Abstract

The global dynamics of the ionized and neutral gases in the environment of Io plays an important role in the interaction of Jupiter's corotating magnetospheric plasma with Io. Stationary simulations of this problem have already been done using the magnetohydrodynamics (MHD) and the electrodynamics approaches. One of the major results of recent simplified two-fluid model simulations [Saur, J., Neubauer, F.M., Strobel, D.F., Summers, M.E., 2002. J. Geophys. Res. 107 (SMP5), 1–18] was the production of the structure of the double-peak in the magnetic field signature of the I0 flyby. These could not be explained before by standard MHD models. In this paper, we present a hybrid simulation for Io with kinetic ions and fluid electrons. This method employs a fluid description for electrons and neutrals, whereas for ions a particle approach is used. We also take into account charge-exchange and photoionization processes and solve self-consistently for electric and magnetic fields. Our model may provide a much more accurate description for the ion dynamics than previous approaches and allows us to account for the realistic anisotropic ion velocity distribution that cannot be done in fluid simulations with isotropic temperatures. The first results of such a simulation of the dynamics of ions in Io's environment are discussed in this paper. Comparison with the Galileo I0 flyby results shows that this approach provides an accurate physical basis for the interaction and can therefore naturally reproduce all the observed salient features.

Keywords: Io; Jupiter; Magnetosphere; Satellites; Atmospheres

1. Introduction

The interaction of the jovian plasma torus with Io is a fundamental problem in magnetospheric physics. The plasma environment near Io was studied in situ by Galileo during the prime mission and the extended Galileo Europa mission including the pass I0 in December 1995, I24 in October 1999, and I27 in February 2000 (Frank et al., 1996; Frank and Paterson, 2000; Kivelson et al., 1996).

The most general and accurate theoretical approach for this problem would require the solution of a non-linear coupled set of integro-MHD/kinetic-Boltzmann equations which describe the dynamics of Jupiter's corotating magnetospheric plasma, pickup ions and the ionosphere together with the neutrals from Io's atmosphere. To leading order, the plasma and neutral atoms and molecules are coupled by charge exchange and ionization. The characteristic scale of the ionized components is usually determined by the typical ion gyroradius, which for Io is much less than characteristic global magnetospheric scales of interest, but the ion gyroradius may be comparable with the size the current sheets near Io. By contrast, the mean free path of neutral particles is comparable to the characteristic exospheric scales such as the thickness of the exosphere or the scale height of the atmosphere of Io. Consequently, the Knudsen number $Kn = \lambda/L_{\mathrm{exo}}$ (λ, the mean free path of neutral particles and L_{exo}, a characteristic exospheric scale), which is a measure of the distribution relaxation distance, satisfies $Kn \ll 1$ inside the exosphere, and $Kn \gg 1$ outside the exosphere. Thus it is gener-

* Corresponding author. Address for correspondence: Department of Physics, The University of Alberta, Edmonton, AB T6G 2J1, Canada. Fax: +1 (780) 492 0714.
E-mail addresses: alipatov@phys.ualberta.ca, lipat@antivir.ru, lip@linmpi.mpg.de (A.S. Lipatov).

0019-1035/$ – see front matter
doi:10.1016/j.icarus.2005.08.012

ally not valid to assume that the distribution of the neutral atoms and ions can relax to a Maxwellian distribution, and one needs ideally to solve a Boltzmann equation for the neutral and ionized components in which charge exchange and photoionization processes are included. This is why kinetic approaches, such as Direct Simulation Monte Carlo have been applied to understand global aspects of the neutral atmosphere (Marconi et al., 1996; Austin and Goldstein, 2000).

Plasma kinetic simulations are, however, much more complicated, and even at the current stage of computational technology require some approximations and compromises to make some initial progress. Several approaches for including the neutral component and pickup ions self-consistently in models describing the interaction of plasma torus with Io have been formulated. Early theoretical work was often done either in the context of a "thin" atmosphere (e.g., see Cloutier et al., 1978) indicative of the surface temperature (130 K), or "thick" extended neutral atmosphere (e.g., see Goertz, 1980) more indicative of volcanic temperatures (1000 K). Subsequent evidence (see the review by Lellouch, 1996) seems to indicate a mixed picture of an irregular global atmosphere, which has a large extended corona like a thick atmosphere, but appears to be dominated by local sublimation and major injection of hot (high speed) gas/dust plumes to high altitudes but only near active volcanic vents. Therefore, although the atmosphere is probably only locally and irregularly thick, it still has a large extended neutral corona which provides a sufficient source of impact ionization and photoionization to explain a spatially extended interaction with the plasma torus.

Southwood et al. (1980) examined data from several Voyager instruments and examined the possible role of an intrinsic magnetic field for Io as a way to retain a robust enough ionosphere, which could provide enough conductivity for completing the Io–Jupiter current circuit. Neubauer (1980) presented an analytical model of the Alfvén standing wave current system which connects current through the ionosphere of Io. Southwood and Dunlop (1984) and Ip (1990) suggested models stating that mass loading effects should result in the formation of a tail-like structure in the wake behind Io; as a consequence of the enhanced plasma density, the magnetic field perturbations are continued into the wake. Thus the field-aligned current is not only generated by Io itself, but also in the wake. This has been born out in Hubble Space Telescope images of the footprint of Io and its wake on Jupiter's ionosphere (Clarke et al., 2002). Several years after Voyager, 3D numerical studies of the plasma flow past Io were performed using electrodynamic (Wolf-Gladrow et al., 1987), magnetohydrodynamic (Linker et al., 1989, 1991) and resistive magnetohydrodynamic (Kopp, 1996; Kopp et al., 1998) approaches.

There have been recent efforts to improve and extend the pre-Galileo simulations both in terms of the MHD (Combi et al., 1998; Linker et al., 1998; Kabin et al., 2001) and the electrodynamic (Saur et al., 1999) approaches. These two approaches are distinguished by the physical assumptions which they each do and do not (or in some cases, can and cannot) include. MHD cannot, at least yet, include the effects of realistic conductivities (Hall and Pedersen) or charge separation effects which are likely to be important very close to Io where the neutral densities are large and the electric potential can introduce non-symmetric flow around body. MHD models either include constant artificial conductivity (Linker et al., 1998) or assume perfect conductivity (Combi et al., 1998). Comparisons of the sets of published results do not indicate that this choice has any important consequence.

The magnetized models of Linker et al. (1998) produced a broad and deep perturbation, but not the self-reversal at the center of the wake (the double-peak or bite-out). Thus, the observational data, e.g., density and magnetic field profile along the Galileo trajectory cannot be fully explained by MHD models. The most recent evidence from all the Galileo flyby data is that Io does not possess any substantial internal magnetic field of its own (Kivelson et al., 2001).

The first electrodynamic models (Saur et al., 1999) produced magnetic field perturbations that are similar to the Galileo measurements, but none are quite as deep or as broad, and none have the reversal of the perturbation (the double-peaked structure) in the center of the wake. In the electrodynamical model of Saur et al. (2002), they added an extra ionization source, based on the high-energy bidirectional electrons observed by Williams et al. (1996, 1999) and Frank and Paterson (1999). These high-energy electrons were included as an energy source in addition to electron impact ionization by the thermal electrons and photoionization to create a dense plasma wake as is observed. Electrodynamic simulations without these extra bidirectional electrons show a nearly empty wake (Saur et al., 1999) and indicate that the electrodynamic part of Io's interaction is best described as an ionosphere-like interaction rather than a comet-like interaction (Saur et al., 2003). Saur et al. (2002) demonstrated that diamagnetic and inertial currents are responsible for formation of the observed double-peak magnetic profile along the I0 trajectory. Their model produced a magnetic field profile with an oscillating structure and a maximum that is narrower than the observations for a standard atmosphere model (Fig. 11 in Saur et al., 2002). When using a longitudinally symmetric atmosphere they obtained a strong double-peaked structure, but the breadth of the structure along the spacecraft trajectory was half the size of that observed (Fig. 14 in Saur et al., 2002) and the amplitude of the peaks was much smaller than observed.

We could go into a litany of the good and bad points of each method. The electrodynamic approach for example is essentially an incompressible fluid with a non-self-consistent B field but includes realistic conductivities and a more self-consistent ionization source. MHD includes a compressible fluid and a self-consistent B field, but uses an imposed ionization distribution and does not include realistic conductivities (this is true even for Kopp's model which claims to be resistive). The electrodynamic approach makes some attempt of dealing with electron temperature for ionization, but does not include its dynamical effects. MHD essentially avoids dealing with electrons except indirectly.

In this paper, we describe a new approach to solving the time-dependent Boltzmann equation (a "particle in cell" approach) together with a hybrid plasma (ion kinetic) model in three spatial dimensions using a prescribed but adjustable neu-

tral atmosphere model for Io. A Boltzmann simulation is applied to model charge exchange between (incoming and pickup) ions and the immobile atmospheric neutrals. Several simulations have been run, and the results described. We show for the first time the predicted distribution for ions and the electromagnetic field throughout Io's environment. The results of these kinetic simulations are compared with those obtained from related MHD models and the Galileo I0 flyby observational data. Through model-data comparison we deduced the best combination of parameters for our model that can satisfactorily reproduce the main behavior of the observational data. Comparison of the results of our hybrid simulation with the Galileo I27 flyby and results of our fluid-ion–particle-ion simulation will be presented in future publication.

2. Formulation of the problem and mathematical model

2.1. Simulation model

To study the interaction of the plasma torus with the ionized and neutral components of Io's environment we use a quasineutral hybrid model for ions and electrons. The model includes ionization, which in the Io environment is dominated by electron impact ionization, not photoionization, and charge exchange. In any case the ionization mechanism is not specified. We explicitly include ionization mass-loading and charge exchange as the dominant mechanisms for the interaction away from the lower boundary at Io, but we include a finite conductivity, given by the diffusion scale length, at the inner boundary. The atmosphere is considered to be an immobile component in this paper.

The general scheme of the global interaction of the plasma torus with Io and the Galileo I0 trajectory is given in Fig. 1. The Galileo I0 flyby occurred nearly in the equator plane of Io and perpendicular to the direction of the plasma wake defined by the corotating plasma flow past Io. The spacecraft trajectory passed approximately 900 km down-stream of Io (in the sense of the plasma torus flow). In our coordinate system the Z axis is parallel to U_0 (corotational plasma velocity), Y is aligned with the spin axis, and $\mathbf{X} = \mathbf{Y} \times \mathbf{Z}$. The relation between our coordinate system and the IphiO (X^*, Y^*, Z^*) system (see Fig. 3 from Kivelson et al., 2001) is the following: X is parallel to Y^*, Y is aligned with Z^*, and Z is parallel to X^*.

In the hybrid simulations described here, the dynamics of upstream ions and implanted ions is described in a kinetic approach, while the dynamics of the electrons is described in a hydrodynamical approximation.

The single particle ion distribution function $f_s(t, \mathbf{x}, \mathbf{v})$ has to fulfill the Vlasov/Boltzmann equation

$$\frac{\partial}{\partial t} f_s + \mathbf{v}\frac{\partial}{\partial \mathbf{x}} f_s + \frac{\mathbf{F}}{M_s}\frac{\partial}{\partial \mathbf{v}} f_s = F_{\text{coll}} + P - L_{\text{exch}}, \tag{1}$$

where $\mathbf{F}$ symbolizes forces due to electric and magnetic fields acting on the ions, F_{coll} is the collision term, P denotes the production rate of the ions by an ionization and charge exchange, and L_{exch} the loss rate of ions due to charge exchange at $(\mathbf{x}, \mathbf{v})$.

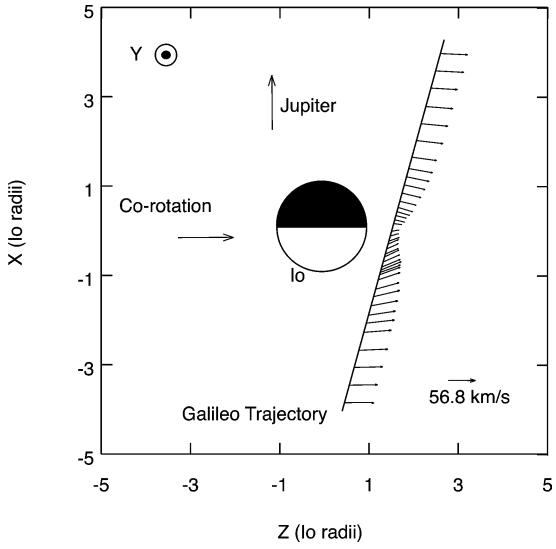

Fig. 1. Galileo trajectory close to Io and the system of coordinates. From Kabin et al. (2001).

In this paper we use the particle-mesh model for ion dynamics instead of the Vlasov/Boltzmann equation, Eq. (1).

The single ion particle motion is described by the equations (see, e.g., Eqs. (1) and (14) from Mankofsky et al., 1987):

$$\begin{aligned}
&\frac{\mathrm{d}\mathbf{r}_{s,l}}{\mathrm{d}t} = \mathbf{v}_{s,l};\\
&\frac{\mathrm{d}\mathbf{v}_{s,l}}{\mathrm{d}t} = \frac{e}{M_\mathrm{i}}\left(\mathbf{E} + \frac{\mathbf{v}_{s,l}\times\mathbf{B}}{c}\right)\\
&\qquad - \frac{m_\mathrm{e}\nu_\mathrm{ie}}{M_\mathrm{i}}(\mathbf{v}_{s,l} - \mathbf{U}_\mathrm{i}) - \frac{m_\mathrm{e}\nu_\mathrm{ie}}{M_\mathrm{i} e n_\mathrm{i}}\mathbf{J} - \nu_\mathrm{io}\mathbf{v}_{s,l}.
\end{aligned} \tag{2}$$

Here we assume that the charge state is $Z_\mathrm{i} = 1$ and that all ions have the same mass M_i. $\mathbf{U}_\mathrm{i}$ and $\mathbf{J}$ denote the charge-averaged velocity of all (incoming and pickup) ions and the total current, Eq. (7). The subscript s denotes the ion population ($s = 1$ for incoming ions and $s = 2$ for pickup ions) and the index l is the particle index. ν_ie and ν_io are collision frequencies between ions and electrons, and ions and neutrals that may include Coulomb collisions and collisions due to particle–wave interaction. Note that the collision rates used in Eq. (2) must depend on individual velocities of ions and electrons. However, we use the effective resistivity η, $\eta = \sigma^{-1} = m_\mathrm{e}/(ne^2\tau_\mathrm{e})$, where $\tau_\mathrm{e} = \nu_\mathrm{ie}^{-1}$. The electrical conductivities may be estimated as

$$\begin{aligned}
&\sigma_\perp = \sigma_1 T_\mathrm{e}^{3/2}, \qquad \sigma_\parallel = 1.92\sigma_\perp,\\
&\sigma_1 = 0.9\times 10^{13}/((\Lambda/10)Z_\mathrm{i})\ \mathrm{s}^{-1}\,\mathrm{eV}^{-3/2},
\end{aligned} \tag{3}$$

where T_e denotes the electron temperature and Λ is the Coulomb logarithm (see, e.g., pp. 215–216 from Braginskii, 1965). For the typical plasma torus parameters $T_\mathrm{e} = 5$ eV (electron temperature) and $n_0 = 3600\ \mathrm{cm}^{-3}$ (density) the electrical conductivities are $\sigma_\perp \approx 4.7\times 10^{13}\ \mathrm{s}^{-1}$ and $\sigma_\parallel \approx 9.2\times 10^{13}\ \mathrm{s}^{-1}$. Charged particle–neutral collision frequencies are calculated depending on the specie in question. For plasma, the thermal velocity, v'_α ($\alpha = i, e$), is assumed greater than the drift velocity, so we take

$$\nu_{\alpha,\mathrm{o}} = n_\mathrm{o}\sigma^{\mathrm{o},\alpha} v'_\alpha, \tag{4}$$

where the cross section $\sigma^{o,\alpha}$ is typically about 5×10^{-15} cm^2 and (see, e.g., Eq. (17) from Mankofsky et al., 1987).

In our simulation we use the low (much smaller that the real value) effective conductivity to suppress "shot" noise and for modeling Io's body; hence, we may drop the first collision term in the right hand side of Eq. (2) for simplicity. We also drop the third collisional term in Eq. (2) for simplicity. We also take into account the interaction of ions with neutral particles by charge exchange (see, Eqs. (13)–(17)). We also assume that the bulk velocity and thermal temperatures of neutral particles equal zero.

In the nonradiative limit Ampère's law is given by

$$\frac{4\pi}{c}\mathbf{J} = \nabla \times \mathbf{B}; \tag{5}$$

and the induction equation (Faraday's law) by

$$\frac{1}{c}\frac{\partial \mathbf{B}}{\partial t} + \nabla \times \mathbf{E} = 0. \tag{6}$$

The total current is given by

$$\mathbf{J} = \mathbf{J}_e + \mathbf{J}_i; \quad \mathbf{J}_i = \sum_{s=1}^{2} e n_s \mathbf{U}_s = e n_i \mathbf{U}_i, \tag{7}$$

where $\mathbf{U}_s$ is the bulk velocity of ions of the type s.

We further assume quasi-neutrality

$$n_e = \sum_{s=1}^{2} n_s. \tag{8}$$

For massless electrons the equation of motion of the electron fluid takes the form of standard generalized Ohm's law (e.g., Braginskii, 1965):

$$\mathbf{E} = \frac{1}{e n_e c}(\mathbf{J}_e \times \mathbf{B}) - \frac{1}{e n_e}\nabla p_e - \frac{m_e}{e}\left[\sum_s \nu_{e,s}\left[(\mathbf{U}_i - \mathbf{U}_s) - \frac{\mathbf{J}}{ne}\right] + \nu_{a,eo}\mathbf{U}_e\right], \tag{9}$$

where $p_e = n m_e \langle v_e'^2 \rangle / 3 = n_e k_B T_e$, and v_e' are the scalar electron pressure and the thermal velocity of electrons, and the electron current is estimated from Eq. (7). The evaluation of the effective conductivities that correspond the frequency $\nu_{e,o}$ gives the following expression

$$\sigma_{e,o} = \frac{\omega_{pe}^2}{4\pi \nu_{e,o}} = \frac{\omega_{pe}^2}{4\pi \sigma^{e,o} v_e'} = \frac{1.64 \times 10^{14} n_e'}{n_o'} \text{ s}^{-1}, \tag{10}$$

where dimensional values are $n_e' = n_e/n_0$ (electron density) and $n_o' = n_o/n_{atmos}$ (neutral density). Here we take $n_0 = 3600$ cm^{-3}, $n_o = 10^9$ cm^{-3} and $v_e' = 40$ km/s. Equation (3) gives $\sigma_{e,i} = 0.4 \times 10^{14}$ s^{-1} for plasma torus parameters. Equation (10) demonstrates that effective conductivity σ_{eo} may exceed the value of σ_{ei} near the Io's surface. In our simulation we assume that $|\mathbf{U}_i - \mathbf{U}_s| \ll J/(ne)$ and we drop the fourth and sixth terms from the right side of Eq. (9).

Since we suppose that electron heating due to collisions with ions is very small, the electron fluid is considered adiabatic. For simplicity we assume that the total electron pressure may be represented as a sum of partial pressures of all electron populations:

$$p_e \propto \frac{(\beta_e n_{i,up}^{5/3} + \beta_{e,PI} n_{i,PI}^{5/3} + \beta_{e,iono} n_{i,iono}^{5/3})}{\beta_e}, \tag{11}$$

where β_e, $\beta_{e,PI}$, and $\beta_{e,iono}$ denote electron upwind, pickup and ionosphere betas. We also assume here that $n_{e,up} = n_{i,up}$, $n_{e,PI} = n_{i,PI}$, and $n_{e,iono} = n_{i,iono}$. Otherwise, we have to calculate the electron pressure from heat balance for electrons (see, e.g., Braginskii, 1965) taking into account the heat fluxes for pickup electrons and ionospheric electrons on the right side of this equation. At this stage of our research we do not yet have a numerical solver for this equation. The ion kinetic approach allows us to take into account the effects of anisotropy of ion pressure, the correct mass loading processes, the penetration of ions across the ionosphere, and the asymmetry of plasma flow around Io. Remember that the fluid models which account only for the scalar (i.e., isotropic) ion pressure may result in an extra-expansion of the pickup ions along the Alfvén wing.

Charge exchange may be included in a hybrid model by a simple procedure (Lipatov et al., 1998; Lipatov, 2002) that was used for the study of the dynamics of an H component inside the heliosphere. The total loss rate in s^{-1} for the ionized component has the form

$$\beta_{ex}(\mathbf{x}, \mathbf{v}, t) = \int f_a(\mathbf{x}, \mathbf{v}_a, t) V_{rel,a} \sigma_{ex}(V_{rel,a})\, \mathrm{d}^3\mathbf{v}_a, \tag{12}$$

where the velocity of ions relative to an atom with velocity $\mathbf{v}_a$ is $V_{rel,a} = |\mathbf{v} - \mathbf{v}_a|$.

If we suppose that the neutral component has a Maxwellian distribution, then β_{ex} may be approximated as (Ripkin and Fahr, 1983)

$$\beta_{ex}(\mathbf{x}, \mathbf{v}, t) \simeq n_a(\mathbf{x}, t) V_{rel,a} \sigma_{ex}(V_{rel,a}). \tag{13}$$

In this paper we assume that the neutral component of Io's atmosphere has zero bulk and thermal velocities. If one needs to include the nonzero temperature and bulk velocity, the effective average velocity of ions relative to an atom with velocity may be found from the general equation of Ripkin and Fahr (1983).

The actions of many real ions (10^{30}–10^{34}) are modeled by following a large but manageably representative sample of (10^7–10^8) simulation particles. At any point in a simulation either when the particles are initially produced or they change direction because of an interaction, it is necessary to account properly for the spatial and/or velocity distribution of the process in question in fair manner. The allowed degrees of freedom of the variable in question are then spanned with a method of random deviates whereby the normalized probability density distribution of the process in question is integrated over all possible values (e.g., directions, velocities, decay times, etc.) and one fair value is chosen by picking a random number on the interval from 0 to 1. One such process is to decide if a simulation ion in question will undergo a charge exchange reaction during its next time step interval.

Let the time interval t^* with respect to the charge exchange be a random variable with a distribution function

$$w_l(t^*) = \exp\left[-\int_{t_0}^{t^*} \beta_{\mathrm{ex},l}\,\mathrm{d}t\right], \tag{14}$$

where l is the particle index.

A survival probability against the charge exchange event, w_{ex}, may be written as follows:

$$w_{\mathrm{ex},l}(t) = \exp\left[-\int_{t_0}^{t} \beta_{\mathrm{ex},l}\,\mathrm{d}t\right]. \tag{15}$$

The integration is over the trajectory of the particle with index l. At the time of creation (either at the boundary of the calculation box, or at the moment of charge exchange), an ionized particle has initial coordinates $\mathbf{x}_l(t_0) = \mathbf{x}_{l,0}$, $\mathbf{v}_l(t_0) = \mathbf{v}_{l,0}$, and a survival probability $w_{\mathrm{ex},l}(t_0) = 1$. For each new ion with index l, we have to determine the critical probability $w^*_{\mathrm{ex},l}$ when charge exchange will occur, and this is done using the relation

$$w^*_{\mathrm{ex},l} = \xi, \tag{16}$$

where ξ is random number on the interval from 0 to 1. During the calculation we have to identify those particles for which the probability of survival satisfies the condition

$$w_{\mathrm{ex},l} \leqslant w^*_{\mathrm{ex},l}. \tag{17}$$

If the particle satisfies the condition (17), then we have to exchange the velocity of this ion with the velocity of an atom from the atmosphere of Io. In the present simulations, we do not take the cross section σ into account in (12) because of the weak dependence on $|v - v_{\mathrm{p}}|$ (as was done in the work of Malama, 1991). If charge exchange occurs, then a new ionized particle begins its motion with $\mathbf{v}_l = 0$ and $w_{\mathrm{ex},l} = 1$.

The neutral atmosphere of Io serves as a source of new ions, mainly by electron impact ionization from corotating (or nearly corotating) plasma and also by photoionization. The neutral atmosphere also serves as collisional targets for charge exchange by corotating ions. The impacting ions consist both of upstream torus ions as well as newly implanted ions which are picked up by the motional electric field. We have adopted a two-component description for the neutral atmosphere of the form

$$n_{\mathrm{neutral}} \approx n_{\mathrm{atmos}}\left(W_{\mathrm{ext}}\frac{H_{\mathrm{atmos}}}{4}\frac{r_{\mathrm{Io}}}{r^2} + W_{\mathrm{int}}\exp\left(-\frac{r - r_{\mathrm{Io}}}{H_{\mathrm{atmos}}}\right)\right), \tag{18}$$

where n_{atmos} denotes the maximum value of the neutral density extrapolated to the surface of Io. Note that since we are limited computationally to cells which are large compared with the scale height of the low altitude cold atmosphere, our value of n_{atmos} is much lower than the true density of SO_2, SO and S_2 near the surface, but it provides a reasonable description of the neutral densities from altitudes of 50 km to several Io radii.

Io's neutral atmosphere is then assumed to be composed of two components: an extended corona or halo distribution based on the first term on the left hand side of Eq. (18) and lower exosphere distribution close to Io. The production of new ions in the extended halo then corresponds to

$$G_{\mathrm{halo}} \propto \nu_{\mathrm{i}} n_{\mathrm{atmos}} W_{\mathrm{ext}} \frac{H_{\mathrm{atmos}}}{4r_{\mathrm{Io}}}\left(\frac{r}{r_{\mathrm{Io}}}\right)^{-2} \tag{19}$$

for $r_{\mathrm{Io}} < r < 7r_{\mathrm{Io}}$, and the production of new ions from the lower exosphere near Io corresponds to

$$G_{\mathrm{exo}} \propto \nu_{\mathrm{i}} n_{\mathrm{atmos}} W_{\mathrm{int}} \exp\left[-(r - r_{\mathrm{Io}})/H_{\mathrm{atmos}}\right]. \tag{20}$$

Here W_{ext} and W_{int} denote the fraction of the total ion production rate in the halo and exosphere, ($W_{\mathrm{int}} = (70\text{–}100)\%$ of the total), respectively, n_{atmos} denotes the maximum atmosphere density, and ν_{i} is the effective ionization rate per atom or molecule. The values of the overall W_{ext} and W_{int}, in addition to the total global ionization rate and the total global charge exchange rate are found by reproducing, as best as possible, the Io Galileo measurements of B field, plasma density and plasma temperature. After much experience in running the model and examining the effects of the values of different parameters on the measured quantities we have been able to adjust those values to obtain an adequate "fit" to the measurements. A small fraction of those runs is described in the following section of the paper.

The total global ion production can be calculated as

$$Q_{\mathrm{ion}} = 4\pi\int_{r_{\mathrm{Io}}}^{r^*} G_{\mathrm{halo}} r^2\,\mathrm{d}r + 4\pi\int_{r_{\mathrm{Io}}}^{r^*} G_{\mathrm{exo}} r^2\,\mathrm{d}r. \tag{21}$$

Here we assume that there is no production for $r > r^* = 5.6r_{\mathrm{Io}}$.

The total charge exchanges (in whole computational domain) for incoming ions, $Q_{\mathrm{p,exch}}$ and pickup ions, $Q_{\mathrm{c,exch}}$ are calculated directly from a charge exchange for each particle with the neutral component of Io.

The inner region of Io's ionosphere is described by immobile ions with the following density distributions:

$$0.5n_{\mathrm{iono}}\exp\left(-(r - r_{\mathrm{Io}})/H_{\mathrm{eff}}\right), \quad \text{for } r > r_{\mathrm{Io}},$$
$$n_{\mathrm{iono}}\left(1 - 0.5\exp\left(-|r - r_{\mathrm{Io}}|/H_{\mathrm{eff}}\right)\right), \quad \text{for } r < r_{\mathrm{Io}}.$$

Note that the inner region of the ionosphere is introduced to avoid the low-density values in the computational cells which overlap the surface of Io. We assume that the incoming flow and the ionosphere have a small effective resistivity to suppress the "shot" noise fluctuations. We also take into account the effect of the finite conductivity of Io's body so that

$$\sigma_{\mathrm{eff}} = \sigma_{\mathrm{up}}, \quad \text{for } r > r_{\mathrm{Io}} + H_{\mathrm{atmos}},$$
$$\sigma_{\mathrm{eff}} = \sigma_{\mathrm{iono}}, \quad \text{for } r_{\mathrm{Io}} < r \leqslant r_{\mathrm{Io}} + H_{\mathrm{atmos}},$$
$$\sigma_{\mathrm{eff}} = \sigma_{\mathrm{Io}}, \quad \text{for } r \leqslant r_{\mathrm{Io}}.$$

Our code solves Eqs. (1)–(6), (7)–(11), (12)–(17) and (19)–(20).

Initially the computational domain contains only supersonic plasma torus flow with a homogeneous spatial distribution and a Maxwellian velocity distribution; the pickup ions have a weak density and spherical spatial distribution. The magnetic field and electric fields are $\mathbf{B} = \mathbf{B}_0$ and $\mathbf{E} = -\mathbf{U}_0 \times \mathbf{B}_0$. Inside Io electromagnetic fields are $\mathbf{E} = 0$ and $\mathbf{B} = \mathbf{B}_0$, and the bulk

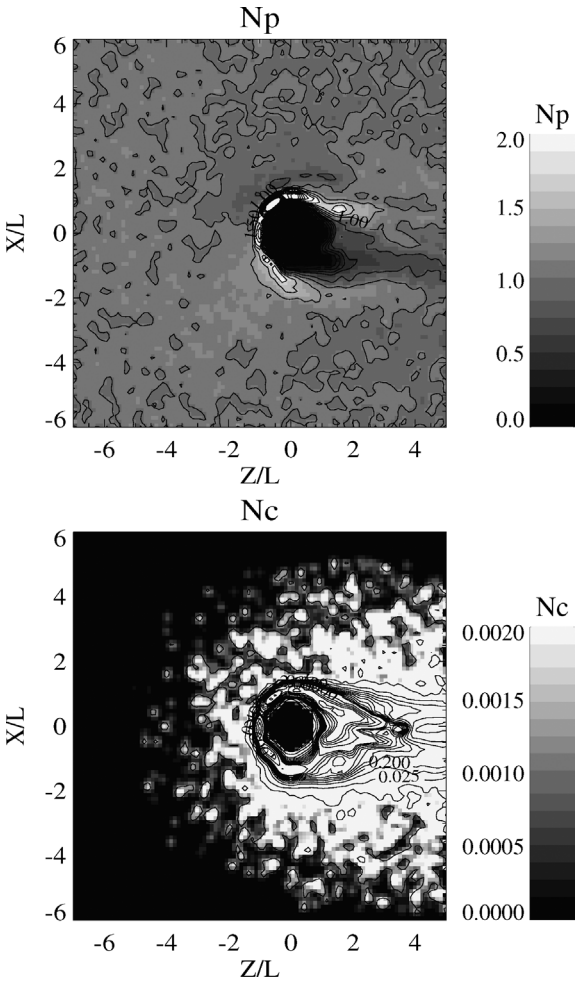

Fig. 2. Incoming (top) and pickup (bottom) ion density in the x–z plane. The case ceie1 (Table 1) with $\beta_{e,PI} = 0.125\beta_e$, $\beta_{e,iono} = 0.125\beta_e$, $W_{ext} = 5\%$, and $H_{atmos} = 0.06$, $l_{d,up} = 0.00125$, $l_{d,iono} = 0.0125$, and $l_{d,Io} = 0.0125$. See explanation in Fig. 6.

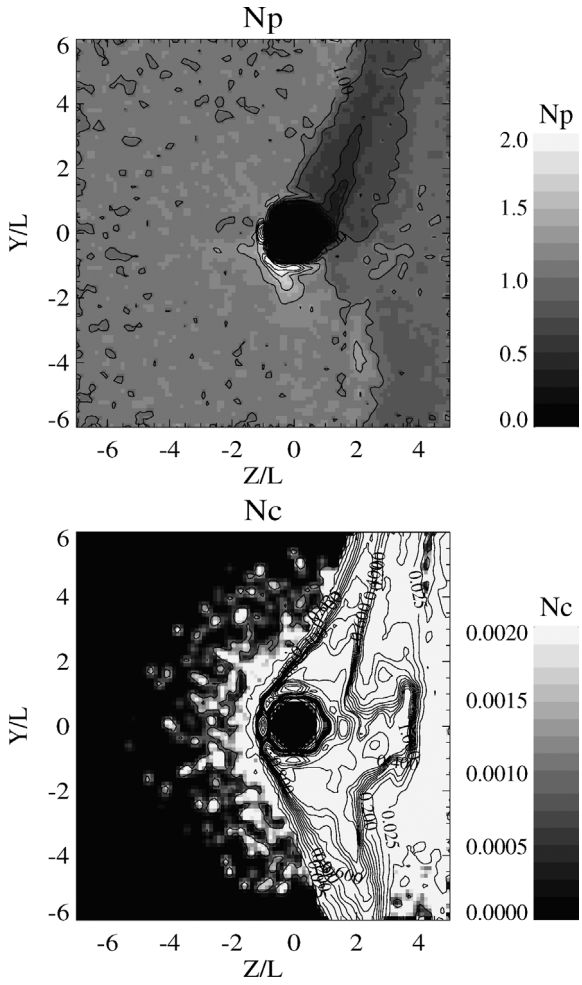

Fig. 3. Incoming (top) and pickup (bottom) ion density in the y–z plane for the same parameters as in Fig. 2. See explanation in Fig. 7.

velocities of ions and electrons are also equal to zero. In the cases examined in Figs. 9–16 we choose $\mathbf{B}_0/B_0 = (0, -1, 0)$, $\mathbf{E}_0/E_0 = (-1, 0, 0)$ and in the cases examined in Figs. 2–8 and 17 we choose $\mathbf{B}_0/B_0 = (0.0394, -0.9854, 0.1657)$ and $\mathbf{E}_0/E_0 = (-0.98, -0.0394, 0.0)$.

At $t > 0$ we begin to inject the pickup ions with a distribution according to Eqs. (19) and (20). Far upstream ($z = -DZ/2$), the ion flux is assumed to have a Maxwellian distribution,

$$f = n_\infty \left(\pi v_{th}^2\right)^{-3/2} \exp\left[-\frac{(\mathbf{v}-\mathbf{U})^2}{2v_{th}^2}\right], \tag{22}$$

where v_{th} and $\mathbf{U}$ are the thermal and the bulk velocities of the plasma torus flow, respectively.

Far downstream, we adopted a free escape condition for particles and Sommerfeld's radiation condition for the magnetic field. On the side boundaries ($y = \pm DY/2$ and $x = \pm DX/2$), periodic boundary conditions were imposed for incoming flow particles and the electromagnetic field. In some cases we also tested the use of the upstream boundary condition for the electromagnetic field on the side boundaries. In these situations we also employed a buffer zone with thickness about of $10 \times \Delta x$, where a smoothing procedure provides a transition for electromagnetic fields from the perturbed value to the upstream value on the side boundaries (see, e.g., Umeda et al., 2001). This effectively allows Io-generated Alfvén disturbances to propagate away. The pickup ions exit the computational domain when they intersect the surfaces $x = 5 \times \Delta x$, $x = DX - 5 \times \Delta x$, $y = 5 \times \Delta y$, $y = DY - 5 \times \Delta y$, $z = 5 \times \Delta z$, $z = DZ - 5 \times \Delta z$. Thus there is no influx of pickup ions at the side boundaries. At Io's surface, $r = r_{Io}$, the particles are reflected (runs in Figs. 9–16) or absorbed (all runs in Table 1). There is no boundary condition for electromagnetic field, and we also use our equations for the electromagnetic field, Eqs. (5), (6) and (9) inside the Io but with internal conductivity and the bulk velocity that is calculated from the particles. In this way the jump in the electric field is due to the variation of the value of the conductivity and bulk velocity across Io's surface. Note that the position of Io is $x = 0$, $y = 0$, $z = 0$.

The three-dimensional computational domain has dimensions $DX = 20L$, $DY = 20L$, and $DZ = 10L$, or $DX = 14L$, $DY = 14L$, and $DZ = 12L$, or $DX = 10L$, $DY = 10L$, and $DZ = 8L$, where L equals the radius of Io, $r_{Io} = 1800$ km. We used meshes of $201 \times 201 \times 101$, or $161 \times 161 \times 121$, or $141 \times 141 \times 121$ grid points, and 2×10^8 and 5×10^7 parti-

cles for ions and pickup ions, respectively, for a homogeneous mesh computation. The time step Δt satisfies the condition $v_{\max}\Delta t \leqslant \min(\Delta x, \Delta y, \Delta z)/8$.

The relationship between dimensional (U, E, B, p_e, n, T) and dimensionless (U', E', B', p'_e, n', T') parameters may be expressed via the dimensional upstream values as follows:

$$\mathbf{U} = \mathbf{U}'U_0, \qquad \mathbf{E} = \mathbf{E}'B_0U_0/c, \qquad \mathbf{B} = \mathbf{B}'B_0,$$
$$p_e = p'_e p_{e0}, \qquad n = n'n_0, \qquad T = T'M_iU_0^2, \tag{23}$$

whereas the dimensional time and distance may be expressed via the bulk velocity U_0 and characteristic scale L:

$$t = t'L/U_0, \qquad x = x'L. \tag{24}$$

The global physics in Io's environment is controlled by a set of dimensionless independent parameters such as M_A, β_i, β_e, M_{PI}/M_p, ion production and charge exchange rates, diffusion lengths, and the ion gyroradius $\epsilon = \rho_{ci}/L$. Here $\rho_{ci} = U_0/(eB/M_ic) = M_Ac/\omega_{pi}$ and the ion plasma frequency $\omega_{pi} = \sqrt{4\pi n_0e^2/M_i}$. For real values of the magnetic field the value of the ion gyroradius is about 8 km which is calculated from the local bulk velocity. The dimensionless ion gyroradius and grid spacing have the values $\epsilon = 0.0045$ and $\Delta_x/L = 0.1$. In order to study the ion kinetic effect, the ion gyroradius has to be resolved on the grid. For this reason it was practically necessary to artificially increase the value of this parameter, $\epsilon = 0.126$, to a value of Δ_x/L. Although this allows us to study the some kinetic effects for realistic physics, we have to extrapolate our results into a realistic scale. By scaling the gyroradius in such a way, we preserve the ratio of M_A, M_S, β_i, β_e, and more importantly accurately preserve any anisotropy of the ion distribution function with respect to the magnetic field. While, in a perfect world it would be better to resolve the physical ion gyroradius, this would require having the linear dimensions of cells be about a factor of ten smaller, which would in turn make the three-dimensional global simulation a 1000 times larger in numbers of particles and computational time. By scaling the gyroradius we can preserve the essential aspects of non-isotropic ion velocity distributions, which is crucial, while accurately modeling all ion creation and collisions rates. These are the most important aspects of the problem. Despite this approximation, the ability to perform a hybrid simulation at all is certainly a major improvement over the isotropic Maxwellian assumptions of all the fluid-based schemes. The only alternative at this time would be to make no progress in this direction.

2.2. Numerical method

We employed a standard particle-in-cell (PIC) method with a homogeneous grid. The time integration of the particle equations of motion uses a leapfrog scheme. The time integration of the electromagnetic field equations uses an implicit finite difference scheme (see, e.g., Lipatov, 2002). We used different time steps for particle and field pushing (subcycling). The code was optimized for parallel computation using MPI and OMP.

Since the gyroradius must be resolved, a grid point spacing of less than 1 gyroradius is required in order to avoid numerical dispersion and dissipation. On the other hand, good statistics are required, therefore a sufficiently large number of particles per cell have to be used (i.e., to obtain low "shot" noise, which manifests itself as fluctuations in the numerical plasma parameters due to a small number of particles per cell).

3. Results of the simulation

To study the interaction of the plasma torus with the ionosphere of Io the following set of jovian plasma torus and ionosphere parameters were adopted in accordance with the Galileo I0 flyby observational data (Frank et al., 1996; Kivelson et al., 1996): corotation velocity, $U_0 = 56.8$ km/s; plasma ion density, $n_0 = 3500\ \mathrm{cm}^{-3}$; plasma temperature, 92 eV; mean ion mass, $M_i = 22M_p$; ratio of specific heats, $\gamma = 5/3$; ion and electron betas, $\beta_i = 0.039$; $\beta_e = 0.0022$; magnetic field, $B = 1800$ nT; Alfvén and sonic Mach numbers $M_A = 0.4$ and $M_S = 2.2$.

For pickup ions we used the following parameters and/or ranges of parameters: total ion production rate, $Q_{ion} = (0.7\text{–}2.0) \times 10^{28}\ \mathrm{s}^{-1}$; mean ion mass, $M_{PI} = 22M_p$; electron pickup and ionosphere betas, $\beta_{e,PI} = 0\text{–}0.0022$, $\beta_{e,iono} = 0\text{–}0.0005$; effective cross section for charge exchange, $\sigma_{exch} = 1.5 \times 10^{-15}\ \mathrm{cm}^2$; atmosphere scale height, $H_{atmos} = (0.06\text{–}0.09) \times r_{Io} = 108\text{–}162$ km; maximum value of the density of the atmosphere, $n_{atmos} = (0.5\text{–}10) \times 10^8\ \mathrm{cm}^{-3}$; effective ionosphere scale height, $H_{eff} = (0.0001\text{–}0.00025) \times r_{Io} = (0.18\text{–}0.45)$ km. Note that in the calculation the effective ionosphere scale height is smoothed over the nearest grid cell and its specific value is not crucial. However, for charge exchange between the ions and atoms we used the analytical formula for the density of the atmosphere without any smoothing. The realistic dimensionless diffusion length in the upstream plasma is about 0.2×10^{-8}, and its value may be higher by factor 10^6–10^7 (see Section 3.4) inside the ionosphere. However, in our simulations we have to choose a much higher effective diffusion length to suppress the numerical "shot" noise. The effective dimensionless diffusion length of the upstream and ionospheric plasmas are $l_{d,up} = 0.00125$, $l_{d,iono} = 0.00125\text{–}0.025$, whereas for Io's body the diffusion length is $l_{d,Io} = 0.0125\text{–}0.025$, where $l_d = 1/Re$ and the magnetic Reynolds number is $Re = 4\pi U_0 L\sigma_{eff}/c^2$. The average Lunquist number for the ionosphere may be estimated as

$$Lq = \frac{\tau_{dif}}{\tau_A} = \frac{Re}{M_A},$$

where the characteristic diffusion and Alfvén times are $\tau_{dif} = 4\pi\sigma L^2/c^2$ and $\tau_A = L/v_A$. Note that Linker et al. (1998) used the following Lundquist number, $Lq = 500\text{–}1000$, magnetic Reynolds number, $Re = 200\text{–}400$ and diffusion length, $l_d = 0.00125$ for the background plasma. This value of the diffusion length corresponds to an effective conductivity of about $0.8 \times 10^8\ \mathrm{s}^{-1}$ far in upstream (in Gaussian units).

Since many plasma and atmospheric parameters are still uncertain we have studied a wide spectrum of simple models in order to choose the best ones for interpretation of the observational data. We can present here only a sample of the wide

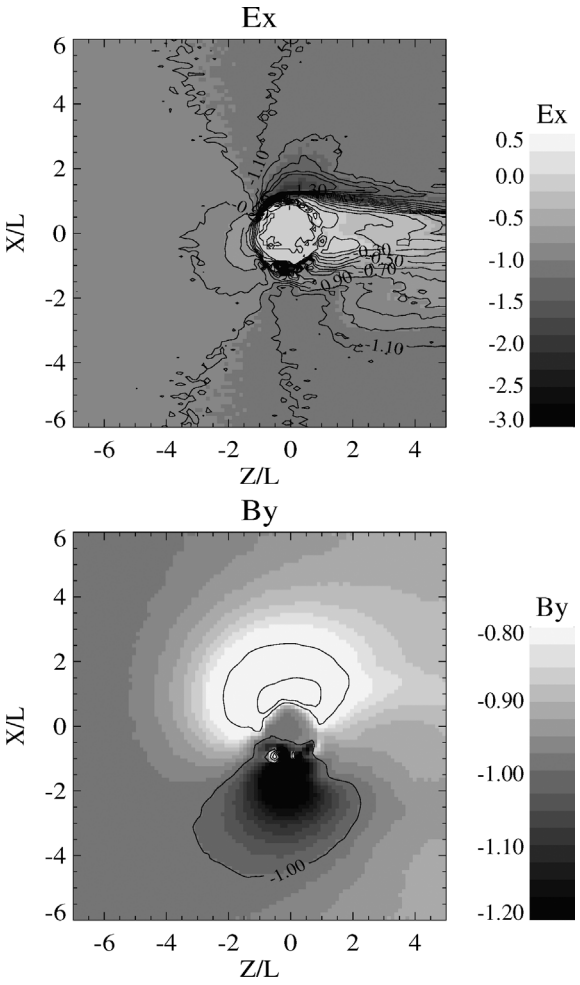

Fig. 4. Electric (top) and magnetic (bottom) fields in the x–z plane for the same parameters as in Fig. 2. Figure shows a strong asymmetry of the electromagnetic field due to finite gyroradius effects.

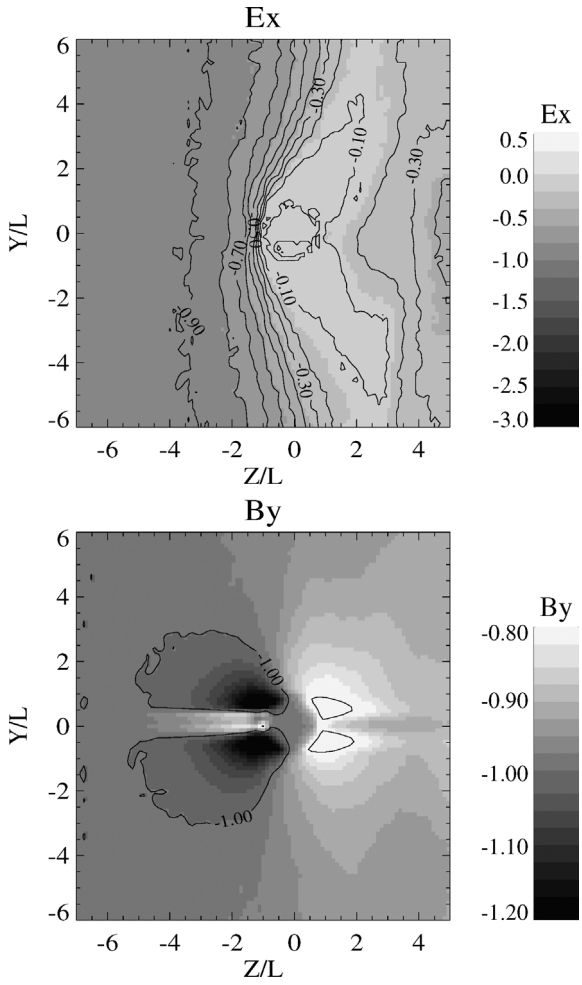

Fig. 5. Electric (top) and magnetic (bottom) fields in the y–z plane for the same parameters as in Fig. 2. Figure shows the formation of an Alfvén wing in the direction of the main magnetic field.

range of simulation results, which we have explored and which were in varying degrees of agreement or disagreement with observations in order to illustrate the dependence of the plasma environment near Io on various values input parameters. We also explored the physical response of the global system to various parameter values and regimes.

3.1. Global structure of Io's environment

Let us consider first the case for the global picture of the interaction of the plasma torus with Io with an ionization rate $Q_{\rm ion} = 3.03 \times 10^{27}\ {\rm s}^{-1}$ (run ceie1, Table 1) and a distribution of neutral component in the form Eq. (18). The maximum value of the atmospheric density is $n_{\rm atmos} = 5 \times 10^{7}\ {\rm cm}^{-3}$ and diffusion lengths are $l_{\rm d,up} = 0.00125$, $l_{\rm d,iono} = 0.0125$, and $l_{\rm d,Io} = 0.0125$. It is worth noting here that clearly our parametrized maximum neutral atmosphere density in combination with our chosen neutral scale height does not represent the actual atmospheric density of SO_2 at the cold surface of Io, but only an extrapolated value which yields a reasonable distribution of neutrals in the 50–400-km region of the atmosphere. Figs. 2 and 3 demonstrate the asymmetrical distribution of the torus plasma ion (top) and pickup ion density (bottom) in the x–z and y–z planes. One can see the increase of the incoming ion density upstream of Io. The pickup ion motion is determined mainly by the electromagnetic drift. The motion along the magnetic field is due to the thermal velocity and the gradient of the electron pressure. The asymmetrical distribution of the incoming ions in the y–z plane may be explained by the existence of the B_z component of the upstream magnetic field. The inclination of the magnetic field results in an asymmetrical boundary condition for ion dynamics (penetration and reflection) in Io's ionosphere and an asymmetrical Alfvén wing.

The pickup ion distribution, Fig. 3 (bottom), gives the correct value for the inclination of the Alfvén wing, 16°–20° for the upper half-wing and 24°–32° for the lower half-wing. If we take into account the inclination of the incoming magnetic field, 10°, these values are in satisfactory agreement with the asymptotic values, 11° and 31°, for $y \to \infty$. The density profile is a little bit disturbed near the side boundaries. However, as already discussed, this perturbation does not affect the region close to Io. Figs. 4 and 5 show the distribution of the electric and magnetic fields. The asymmetry of the distributions in **E** and **B** appears to be caused by the finite gyroradius effects of incom-

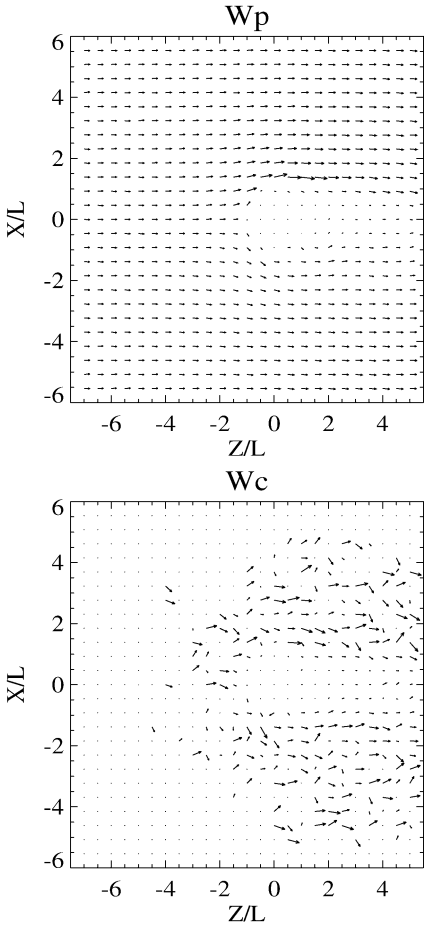

Fig. 6. Incoming (top) and pickup (bottom) ion velocity arrows in the x–z plane for the same parameters as in Fig. 2. The figure demonstrates a flow of pickup ions from the "corona" across the magnetic field. The incoming ions flow around the effective obstacle that is produced by pickup ions and ionosphere.

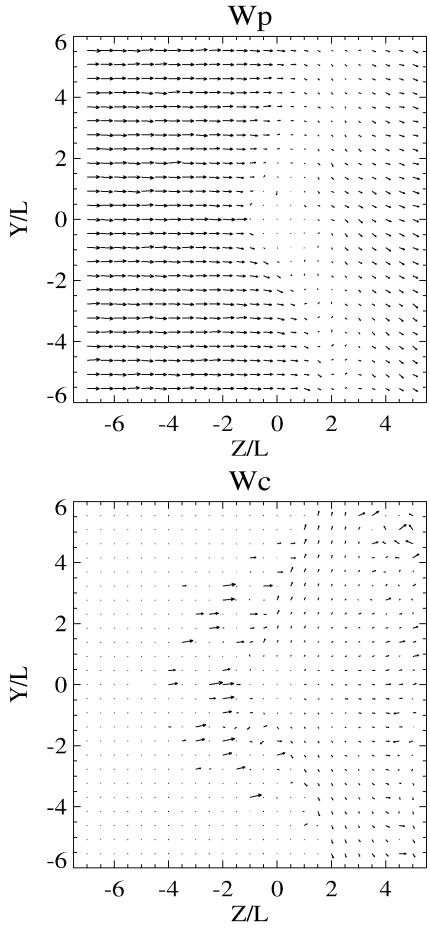

Fig. 7. Incoming (top) and pickup (bottom) ion velocity arrows in the y–z plane for the same parameters as in Fig. 2. The figure demonstrates a strong expansion of pickup ion "corona" along the magnetic field line. The incoming ions flow around the region of extended "corona."

ing and pickup ions. A weak perturbation of the magnetic field was observed near the ionosphere of Io: compression of the upstream magnetic field and decompression in the plasma wake.

Fig. 5 also shows the formation of a strong Alfvén wing in the direction of the magnetic field. Note that the whistler was observed as a leading of a wing at the early time of simulation. Once the simulation stabilized it was replaced by an Alfvén wave. The perturbation of the electric field inside the wings is very strong, and it may affect ion dynamics so that particles flow around the wings. The formation of the Alfvén wing in a sub-Alfvénic flow near Io was studied first analytically by Neubauer (1980). The excitation of a whistler wave near a plasma cloud was studied by using a 3D hybrid simulation by Lipatov (2002). The above wave propagation is closely connected with the generation of low-frequency waves by the magnetic harmonic dipole (local source) in the magnetized plasma. The first analytical studies of these effects may be found, for example, in the work by Van'yan and Lipatov (1972, and references therein).

The arrows in Figs. 6 and 7 show the incoming and pickup ion velocities. The incoming ions flow around the effective obstacle that is produced by pickup ions and the ionosphere. The pickup ions flow from the "corona" across the magnetic field

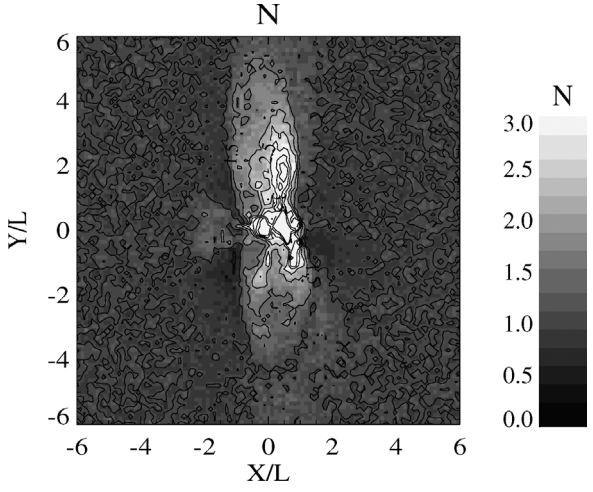

Fig. 8. Two-dimensional cross section for total density in the x–y plane at $z = 1.5r_{\mathrm{Io}}$ for the same parameters as in Fig. 2.

due to electromagnetic drift, whereas the motion along the magnetic field is determined by the thermal velocity of ions and the electron pressure. Fig. 8 shows a two-dimensional cross section cut of total ion density in the x–y plane. One can see the asym-

metry in the distribution relative to the x-axis due to the angle between the bulk velocity and the upstream magnetic field and to the y-axis due to effects of the finite ion gyroradius.

3.2. Effect of electron temperature on the plasma environment

Our model takes into account the physical effects of the temperatures of three characteristic populations of electrons that have not been considered before in past MHD models: (a) the electron population in the plasma torus, T_e; (b) the electron population that is created together with pickup ions, $T_{e,PI}$; (c) the electron population that is created with ions in the ionosphere, $T_{e,iono}$. In accordance with our assumption about the partial pressures of electron populations, we chose the following values for electron temperatures in these simulations: $T_e \propto \beta_e$, $T_{e,PI} \propto \beta_{e,PI} = \beta_e$, and $T_{e,iono} \propto \beta_{e,iono} = 0.25\beta_e$. The value of $\beta_{e,iono}$ was estimated from Fig. 12 (Saur et al., 1999). Note that for the cases discussed in this section the pickup ions are generated only in the exosphere, i.e., $W_{ext} = 0$.

Let us consider case (a). Fig. 9 shows one-dimensional cuts of the total ion density, temperature and magnetic field along the x-axis for $z = 1.5r_{Io}$ and $y = 0$. One can see two peaks in the distribution of the density, each of which has a width of about r_{Io} and maximum densities of about 4 and 6.5 relative to the upstream density. The depletion of the density at $x = 2L$ may be explained as follows. When the supersonic flow passes around the obstacle, a wake with a decreased density is formed. A simple example of a such void is the lunar plasma wake. However, in our case an asymmetrical pickup ion high density obstacle provides an asymmetrical void in Io's plasma wake.

The temperature profile has two peaks with maximum temperatures of about 2.3 and 0.7. These peaks do not correlate with the peak in density because the temperature of the ions is determined by the heated ions from the incoming flow and pickup ions. The magnetic field profile shows a decrease with a minimum value of about 0.5 in the plasma wake and with some significant oscillations (Fig. 9). Fig. 10 shows a two-dimensional cross section of the total ion density across the plasma wake ($z = 1.5r_{Io}$). One can see three strong maxima. This distribution is determined by finite ion gyroradius effects.

If we take into account the temperature of the electron population that is created with the pickup ions (case (b)), the distribution of the ions in the plasma wake is changed significantly. The one-dimensional total density profile has one peak with a value of about 8 (Fig. 11). The temperature profile also has one strong peak with a value of about 1.9, and the magnetic field has a depletion with a minimum value 0.7 (Fig. 11). Fig. 12 shows a two-dimensional cross section of the total density across the plasma wake. One can see a strong peak narrow in x-direction and wide in y-direction.

In case (c), when the temperature of electrons produced inside the ionosphere is also taken into account, we have the following distribution of plasma properties in the wake. Fig. 13 shows one-dimensional cuts of the total density, temperature and magnetic field. The density profile has a wide peak with a thickness of about $4r_{Io}$ and a peak value of $n \approx 6$. The temperature profile has a two-peak distribution. The values of the

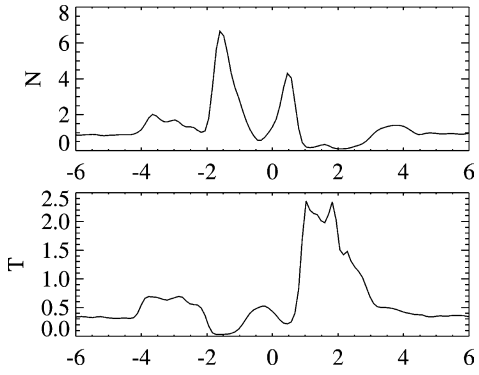

Fig. 9. Total density, temperature and magnetic field along the x-axis at $z = 1.5r_{Io}$. The case with $\beta_{e,PI} = 0$, $\beta_{e,iono} = 0$, $W_{ext} = 0\%$, and $H_{atmos} = 0.06$.

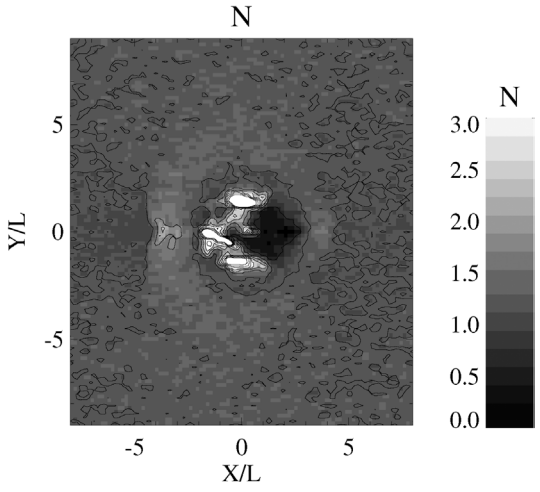

Fig. 10. Two-dimensional cross section for total density in the x–y plane at $z = 1.5r_{Io}$. The case with $\beta_{e,PI} = 0$, $\beta_{e,iono} = 0$, $W_{ext} = 0\%$, and $H_{atmos} = 0.06$.

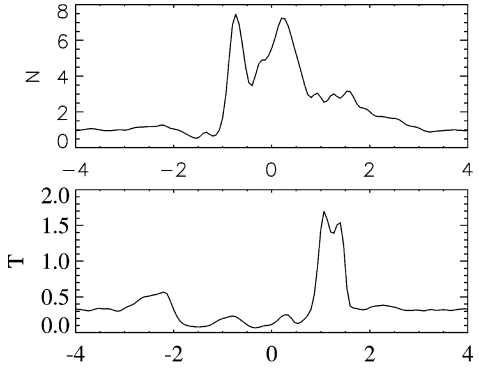

Fig. 11. Total density, temperature and magnetic field along the x-axis at $z = 1.5r_{Io}$. The case with $\beta_{e,PI} = \beta_e$, $\beta_{e,iono} = 0$, $W_{ext} = 0\%$, and $H_{atmos} = 0.06$.

temperature at the two peaks are about 0.6 and 0.55 relative to the upstream value of 0.3. The peaks are separated by a distance of $4r_{Io}$. The magnetic field profile has a minimum at the plasma wake with $B = 0.55$ (Fig. 13). Fig. 14 shows the two-dimensional cross section of the total density across the plasma wake. One can see a strong peak which is narrow in the y-direction and wide in the x-direction. By introducing cool electrons inside the ionosphere we are trying to account in

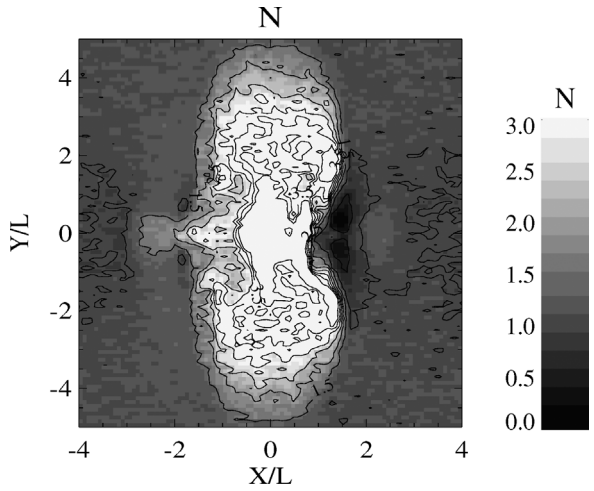

Fig. 12. Two-dimensional cross section for total density in the x–y plane at $z = 1.5r_{\rm Io}$. The case with $\beta_{\rm e,PI} = \beta_{\rm e}$, $\beta_{\rm e,iono} = 0$, $W_{\rm ext} = 0\%$, and $H_{\rm atmos} = 0.06$.

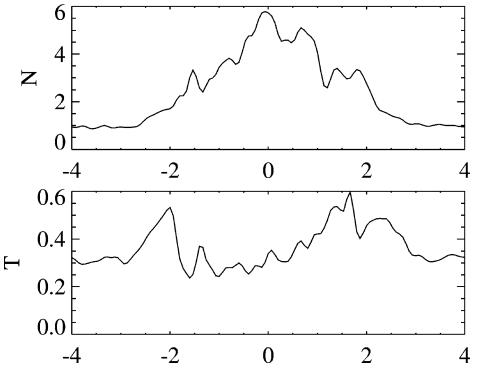

Fig. 13. Total density, temperature and magnetic field along the x-axis at $z = 1.5r_{\rm Io}$. The case with $\beta_{\rm e,PI} = \beta_{\rm e}$, $\beta_{\rm e,iono} = \beta_{\rm e}$, $W_{\rm ext} = 0\%$, $H_{\rm atmos} = 0.06$.

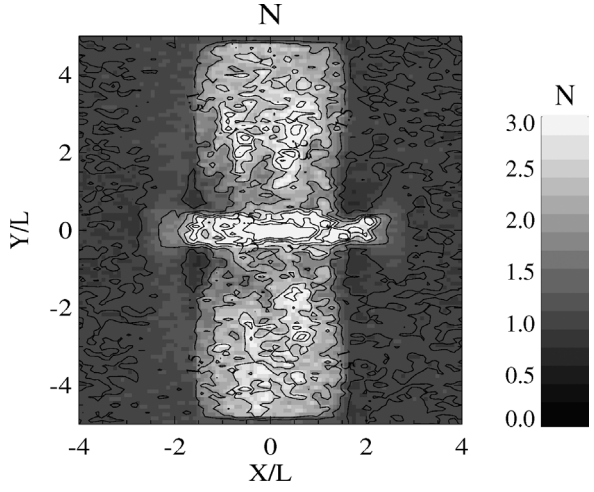

Fig. 14. Two-dimensional cross section for total density in the x–y plane at $z = 1.5r_{\rm Io}$. The case with $\beta_{\rm e,PI} = \beta_{\rm e}$, $\beta_{\rm e,iono} = \beta_{\rm e}$, $W_{\rm ext} = 0\%$, $H_{\rm atmos} = 0.06$.

an appropriate way for the cooling effect on electrons through electron–neutral collisions close to Io.

Finally, we show the two-dimensional cuts of pickup ion density for all three cases, Fig. 15 (top, middle, bottom). One can see that the temperatures of the electron populations

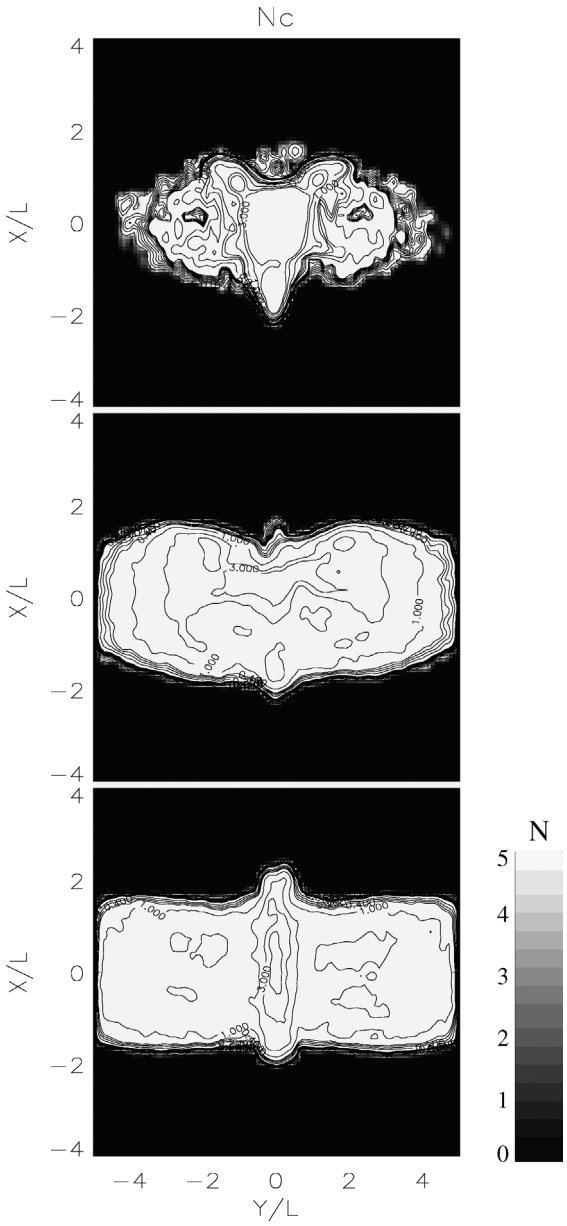

Fig. 15. Two-dimensional cross sections for pickup ion density in the x–y plane at $z = 1.5r_{\rm Io}$. The cases with (top) $\beta_{\rm e,PI} = 0$, $\beta_{\rm e,iono} = 0$; (middle) $\beta_{\rm e,PI} = \beta_{\rm e}$, $\beta_{\rm e,iono} = 0$; (bottom) $\beta_{\rm e,PI} = \beta_{\rm e}$, $\beta_{\rm e,iono} = 0.25\beta_{\rm e}$. $W_{\rm ext} = 0\%$, and $H_{\rm atmos} = 0.06$. Fig. demonstrates asymmetry of pickup ion density across the wake.

which are created in different regions of Io's environment may strongly affect the global ion distribution. Fig. 15 demonstrates the importance of the electron pressure in the region close to Io.

In the absence of pickup and ionospheric electron pressure, the interaction of the plasma torus ions with Io is strongly asymmetrical in the x–z plane due to the finite ion gyroradius. In the plasma wake a "space-mixing" of the pickup ions is observed that results in the formation of an asymmetrical tongue-type distribution in the x–z plane. The effusion of pickup ions in the y-direction is also weak because of small values of $\Delta p_{\rm e}$ and the velocity of the pickup ions in y-direction, Fig. 15 (top).

In the opposite case, when the gradient of the pressure of the pickup electron population and the pressure of the

ionospheric electron population causes a strong electrostatic field, the pickup ion density distribution in the x–z plane becomes more symmetrical and wider across the wake compared with the above case (cf. Fig. 15 (top and bottom)). The gradient of the electron pressure also causes a strong effusion of the pickup ions along the Alfvén wing (see Fig. 15 (bottom and top)).

Finally, in the intermediate case when the pressure of the ionospheric electron population is small, an asymmetrical distribution of pickup ion density with strong effusion along the Alfvén wing is observed, Fig. 15 (middle). So, we can conclude that the pressure of the pickup ions is responsible for effusion processes while the pressure of the ionospheric electron population is responsible for the formation of a symmetrical distribution with the maximum in density located near the ($y = 0$) plane.

All three cases, (a), (b) and (c), demonstrate strong asymmetries in the distributions of pickup ion density, temperature and magnetic field in comparison with MHD and electrodynamic models.

3.3. *Effect of the distribution in pickup ion injection on the plasma environment*

To study the role of pickup ions from the halo we simulated Io's environment for cases when the ion production rate in the halo corresponds to $W_{\rm ext} = 10\%$ and $W_{\rm ext} = 30\%$ of the total (halo plus exosphere) ion production rate. Note that all other parameters are the same in these cases.

Fig. 16 (solid line) presents one-dimensional cuts for density, temperature and magnetic field for $W_{\rm ext} = 10\%$ and $\beta_{\rm e,iono} = 0.25\beta_{\rm e}$. The value of $\beta_{\rm e,iono}$ was estimated from Saur et al. (1999). The density profile has a maximum value of about $n \approx 7.2$, that is larger than the observed value, $n \approx 5.1$, and has a characteristic width of the peak of $3r_{\rm Io}$. The temperature profile shows a two-peak distribution. The maximum values in the peaks are $T/T_0 \approx 3$ and $T/T_0 \approx 2.1$ that correspond reasonably well to the observational data (Frank et al., 1996). The distance between peaks is about $3r_{\rm Io}$ that is a little bit wider than observed value, $2r_{\rm Io}$. The magnetic field profile has a minimum value in the plasma wake of $B \approx 0.5$ that also corresponds to the minimum value of the B_y in the observational data (Kivelson et al., 1996). Fig. 16 (dotted line) shows the one-dimensional cuts for density, temperature and magnetic field for $W_{\rm ext} = 30\%$. The density profile has a maximum value of about $n \approx 5.83$ with a characteristic width of the peak of $4r_{\rm Io}$, which is a little bit wider than that in Fig. 16 (solid line) and is a little higher than observed. The temperature profile also shows a two-peak distribution. The maximum values in the peaks are $T/T_0 \approx 6.8$ and $T/T_0 \approx 2.4$. Note that the first maximum in the temperature is higher than observed (Frank et al., 1996; Kivelson et al., 1996). The magnetic field profile shows a minimum value of the magnetic field in the plasma wake $B \approx 0.56$ that corresponds the observational data.

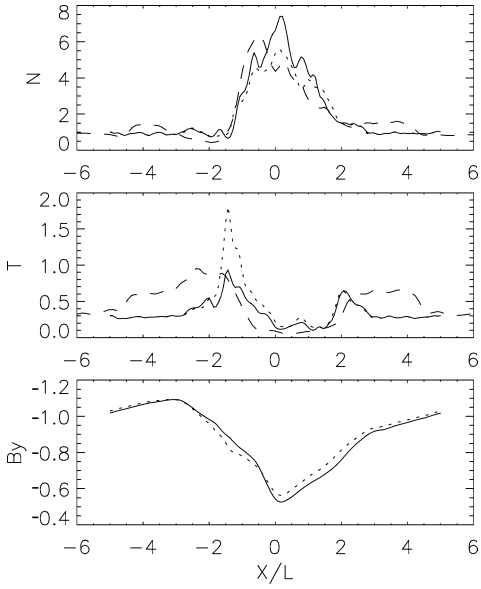

Fig. 16. Total density, temperature and magnetic field along the x-axis at $z = 1.5r_{\rm Io}$ for cases with $\beta_{\rm e,PI} = \beta_{\rm e}$, $\beta_{\rm e,iono} = 0.25\beta_{\rm e}$, $H_{\rm atmos} = 0.06$, $l_{\rm d,up} = 0.0025$; (solid line) $W_{\rm ext} = 10\%$, $l_{\rm d,iono} = 0.0025$; (dotted line) $W_{\rm ext} = 30\%$, $l_{\rm d,iono} = 0.0025$; (dashed line) $W_{\rm ext} = 10\%$, $l_{\rm d,iono} = 0.025$.

3.4. *Effect of ionospheric conductivity on the plasma environment*

In the previous cases we have assumed a high conductivity for the ionosphere and Io's body. Realistic models of Io could include a conducting core, surrounded by a poorly conducting mantle (a Moon-like model), or Io may be considered as a poorly conducting body throughout. In this section we shall model Io as a poorly conducting body. We may estimate the values of the effective conductivity inside the ionosphere of Io by the following expression for the Pedersen conductivity, σ_1 and the Hall conductivity, σ_2 (Saur et al., 1999):

$$\sigma_1 = \frac{en}{B}\frac{\omega_{\rm ci}\nu_{\rm i,o}}{\omega_{\rm ci}^2 + \nu_{\rm i,o}^2} = \frac{\omega_{\rm pi}^2}{4\pi}\frac{\nu_{\rm i,o}}{\omega_{\rm ci}^2 + \nu_{\rm i,o}^2}$$

and

$$\sigma_2 = \frac{en}{B}\frac{\nu_{\rm i,o}^2}{\omega_{\rm ci}^2 + \nu_{\rm i,o}^2} = \frac{\omega_{\rm pi}^2\omega_{\rm ci}}{4\pi}\frac{\nu_{\rm i,o}^2}{\omega_{\rm ci}^2 + \nu_{\rm i,o}^2}.$$

For our assumed parameters of the ionosphere and atmosphere of Io we obtain

$$\sigma_1 \approx 4.8 \times 10^6\text{–}2 \times 10^7\ {\rm s}^{-1}$$

and

$$\sigma_2 \approx 6 \times 10^5\text{–}2.4 \times 10^7\ {\rm s}^{-1}.$$

The above formula gives the value of the effective diffusion length, $l_{\rm d,iono} = 0.0046$–0.02.

Let us consider now the results of a simulation with a high ionospheric conductivity. Note that all other parameters in this case are the same as that shown in Fig. 16 (solid line) except that a higher diffusion length is used, $l_{\rm d,iono} = 0.0125$–0.025.

Fig. 16 (dashed line) shows one-dimensional cuts of the density, temperature and magnetic field for the case with a larger diffusion length, $l_{\mathrm{d,iono}} = 0.025$. The value of the peak density is about $n \approx 7.5$ with the same thickness of the peak, $\approx 3r_{\mathrm{Io}}$, as in the case with a small diffusion length, i.e., high conductivity. The maximum values of the peak temperature, 3 and 2 are approximately the same in either case. However, the magnetic field profile shows much stronger field variation in the external region of the plasma wake in the lower conductivity case. The analysis of the magnetic field inside Io shows that the reduced conductivity ($l_{\mathrm{d,iono}} = 0.025$, Fig. 16 (dashed line)) near the ionosphere and inside Io may reduce the magnetic field inside Io by 20–40%, but the peak plasma density at the Galileo trajectory is only reduced by 5% in comparison with the model with high conductivity.

3.5. Comparison with Galileo observational data

The results of the measurements by the particles and field instruments on the Galileo Orbiter during the December 1995 flyby of Io provided new and important information with which realistic simulations for the plasma interaction can be tested. Along that trajectory physical signatures of the wake were seen as a broad depression in the magnetic field (Kivelson et al., 1996), sharp peaks in the ion (Frank et al., 1996) and electron (Gurnett et al., 1996) densities, a slowing of the plasma in the core of the wake, a deep ion temperature decrease in the center of the wake, and a large (factor of 3) ion temperature rise in the flanks of the wake (Frank et al., 1996). The magnetic field perturbation was broader spatially than the density peak, and showed a double-reversed structure, whereby the perturbation (as defined by the difference from the outer jovian B-field value) was actually weaker right near the close-approach point than it was somewhat adjacent to the center of the wake. For comparison of our computational model with the observational data we made a run with the following plasma parameters: $\beta_{\mathrm{e,PI}} = 0.125\beta_{\mathrm{e}}$, $\beta_{\mathrm{e,iono}} = 0.125\beta_{\mathrm{e}}$, $n_{\mathrm{iono}} = 800n_0$, $H_{\mathrm{atmos}} = 0.06r_{\mathrm{Io}}$, $W_{\mathrm{ext}} = 5\%$, $l_{\mathrm{d,up}} = 0.00125$, and $l_{\mathrm{d,iono}} = 0.0125$. The conductivity of Io is chosen so that $l_{\mathrm{d,Io}} = 0.0125$.

Let us consider first a case in the absence of charge exchange processes (case nce Table 1). The total ion production rate was $Q_{\mathrm{ion}} = 4.8 \times 10^{27}\ \mathrm{s}^{-1}$. Fig. 17 (solid line) shows the comparison of plasma parameters and magnetic field components from the simulation model and observations along the Galileo trajectory (Pass I0). Note that we interpolated the grid values of the plasma parameters and the magnetic field onto the positions of the Galileo spacecraft. We can see that the density peak is slightly shifted to the right in comparison to the observed one. The left peak in the temperature profile is a little bit narrower than the observed one while the right peak is a little bit higher than the observed one. The simulation yields a somewhat smaller value of B_y at large x, $x \gg r_{\mathrm{Io}}$, due to perturbation of the electromagnetic field in the region above ($y > 0$) and below ($y < 0$) the equatorial plane. Unlike the MHD models, the hybrid model yields a B_y profile with a reverse structure in the middle of the plasma wake. This type of behavior may be explained by the diamagnetic and accelerational drift currents in the plasma wake, which are modeled naturally in our kinetic description for the ions. The maximum value of these currents is located near the equatorial plane in the boundary layer (interface) between the external plasma flow and the pickup ions in the plasma wake. The B_z profiles in these simulations correspond very well to the observed data. However, the left maximum in the magnetic field is smaller than the observed one. Unfortunately fluctuations in the magnetic field components are not very small due to "shot" noise in our simulation. So the lack of perfect agreement between observed and computed values of B_x is probably just the result of less than a perfect plasma simulation model ("shot" noise) and the simplified models of the ionosphere and Io's body.

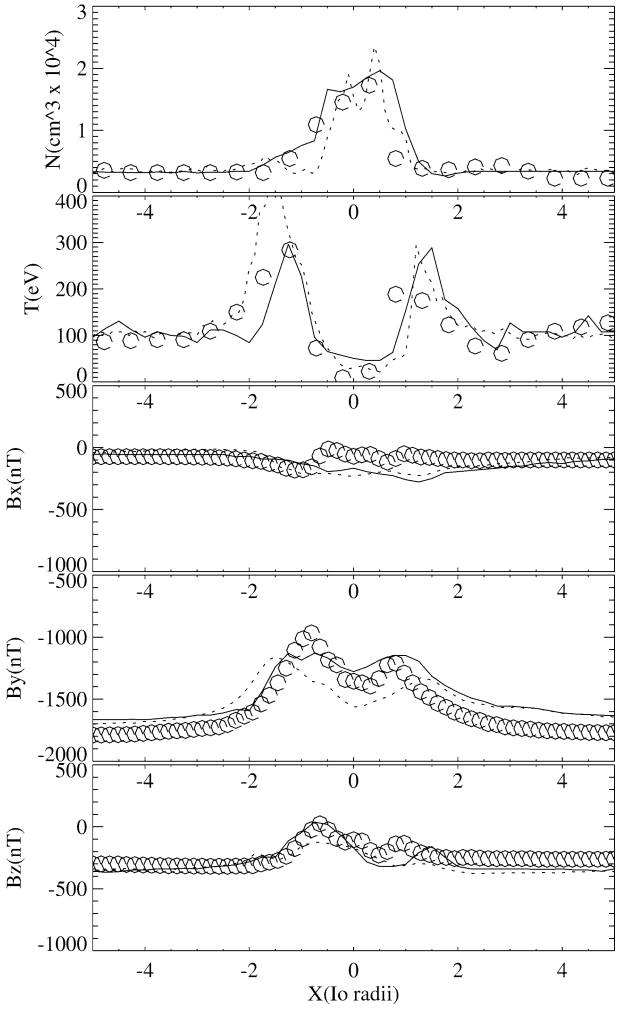

Fig. 17. Comparison of Galileo PLS (I0 pass) (Frank et al., 1996) and MAG (Kivelson et al., 1996) (the open circles) data with the Io hybrid model results along the trajectory for cases with $\beta_{\mathrm{e,PI}} = 0.125\beta_{\mathrm{e}}$, $\beta_{\mathrm{e,iono}} = 0.125\beta_{\mathrm{e}}$, $W_{\mathrm{ext}} = 5\%$, $H_{\mathrm{atmos}} = 0.06$, $n_{\mathrm{iono}} = 800n_0$, and $l_{\mathrm{d,up}} = 0.00125$, $l_{\mathrm{d,iono}} = 0.0125$, and $l_{\mathrm{d,Io}} = 0.0125$: (solid line, case nce, Table 1) in the absence of charge exchange; (dotted line, case ceie1, Table 1) with distribution of the neutral component in form ($n_{\mathrm{neutral}} \approx n_{\mathrm{atmos}}(W_{\mathrm{ext}}(H_{\mathrm{atmos}}/4)(r_{\mathrm{Io}}/r)^2 + W_{\mathrm{int}} \exp(-(r - r_{\mathrm{Io}})/H_{\mathrm{atmos}}))$, $n_{\mathrm{atmos}} = 0.5 \times 10^8\ \mathrm{cm}^{-3}$.

Let us consider now the cases with a charge exchange rate that corresponds to the maximum value of the density of the atmosphere, $n_{\mathrm{atmos}} = 10^8\ \mathrm{cm}^{-3}$. We assume here that the charge

Table 1
Dependence of torus ion charge exchange rate and pickup ion charge exchange rate versus the maximum value of atmospherical density and ionization rate ($Q_0 = 10^{27}$ s^{-1})

Case	$n_{atmos}/10^8$ cm^{-3}	Q_{ion}/Q_0	$Q_{p,exch}/Q_0$	$Q_{c,exch}/Q_0$	Comments
			Model without charge exchange		
nce		4.8	0	0	Density peak is in good agreement with observations, the profile is too wide. Temperature and magnetic field are in a good agreement with observations, Fig. 17.
			Models with charge exchange ($n_{neutral} \approx n_{atmos} \exp(-(r - r_{Io})/H_{atmos})$)		
cei1	1	2.27			Density, temperature and B_y in satisfactory agreement with observations.
cei2	1	2.57			Density and temperature in satisfactory agreement with observations, B_y component is weaker than observed.
cei3	5	2.1			Density in good agreement with observations; temperature and B_y are not.
cei4	10	1.4	12.6	14	Density with strong narrow peak, temperature in satisfactory agreement with observations; B_y is weaker than observed.
cei5	10	2.1	12	20.2	Density with two peaks, temperature is in satisfactory agreement with observation; B_y has much stronger depletion than observed.
			Models with charge exchange ($n_{neutral} \approx n_{atmos}(W_{ext}(H_{atmos}/4)(r_{Io}/r)^2 + W_{int} \exp(-(r - r_{Io})/H_{atmos}))$)		
ceie1	0.5	3.03	3.169	3.13	Density, temperature and B_y in good agreement with observations, Fig. 17.
ceie2	0.5	4.04	2.67	3.87	Density and temperature in satisfactory agreement with observations, B_y is a weaker than observed.
ceie3	1	3.03	5.27	5.6	Density is higher than the observations, variation in B_y is a weaker than observed.
ceie4	1	4.04	5.55	7.93	Density is higher than observations, variation in B_y is weaker than observed.
ceie5	5	4.04	18.3	39.7	Density is much higher than in an observations, variation in the B_y is strong but profile is wider than observed.
ceie6	10	2.1	29.5	37.5	Two-peak density profile, variation in the B_y is much stronger than observed.
ceie7	10	3.03	28.	44.8	Density is much higher than in observations, variation in the B_y is much weaker than observed.
ceie8	10	4.04	27.5	60.	Density is much higher than in observations, variation in B_y is much weaker than observed.

exchange process is due to only the exponential (lower) part of the neutral atmosphere.

In the case where $Q_{ion} = 2.27 \times 10^{27}$ s^{-1} (case cei1, Table 1), the density profile has a smaller effective value but the total temperature is a little bit higher. The left peak in the temperature profile is also a little bit narrower than in the observational data while the right peak is a little bit higher than the observed one. The perturbation in B_y is a little bit smaller than in the case with no charge exchange.

In the case with higher total ion production rate, $Q_{ion} = 2.57 \times 10^{27}$ s^{-1} (case cei2, Table 1) the density profile has a higher effective value but the total temperature is a little bit lower. We can see that the density profile is depleted on the left side and the width of the peak is smaller compared with the case without charge exchange. The left peak in the temperature profile is also a little bit narrower than in the observational data while the right peak is a little bit higher than the observed one. The perturbation in B_y is a little bit smaller than in the case without charge exchange.

In previous cases we assumed that the charge exchange process is only due to the lower altitude, exponential part of the neutral atmosphere. Let us consider now the results of a simulation that also includes the charge exchange due to the extended atmosphere which is distributed as r^{-2} (cases ceie1–ceie8, Table 1).

Let us consider first the cases with a low maximum value of the density of atmosphere, $n_{atmos} = 5 \times 10^7$ cm^{-3}, and an ionization rate of $Q_{ion} = (3.03\text{–}4.04) \times 10^{27}$ s^{-1}. In the case with a lower ionization rate, $Q_{ion} = 3.03 \times 10^{27}$ s^{-1}, the density profile is in agreement with the observation, but the temperature is a little bit higher in the peaks (Fig. 17, dotted line). The magnetic field profile (B_y) is in a qualitative agreement with the observation (Fig. 17, dotted line). In the case with a higher ionization rate, $Q_{ion} = 4.04 \times 10^{27}$ s^{-1}, the density profile is a little bit higher in peak than the observed one and the temperature is a little bit lower in the left peak. The magnetic field profile (B_y) is much smoother than in the observation (not shown in Fig. 17).

One of the main issues in the plasma torus–Io interaction is the question about the real obstacle in this interaction. There are two possible candidates—(1) mass loading by the pickup ions originally produced from Io's atmosphere by the ionization or charge exchange processes between the incoming plasma torus ions and the neutral atmosphere, or (2) charge exchange processes between the pickup ions originally produced in Io's atmosphere and the neutral atmosphere. Table 1 gives a summary of the results of the simulations for the various models that are discussed here.

In the case with a high density for Io's atmosphere (10^9 cm^{-3}), the charge exchange rate becomes very high, $Q_{exch} \approx (6.7\text{–}9) \times 10^{28}$ s^{-1} (cases ceie6, ceie7 and ceie8, Table 1). Note that in these cases the charge exchange rate for incoming ions is much smaller than for pickup ions. We also compared the charge exchange rates in the external ($r > r_{Io} + 4H_{atmos}$) and the internal ($r \leqslant r_{Io} + 4H_{atmos}$) regions separately. The charge

exchange rate for incoming ions in the external region has approximately the same value as the charge exchange rate in the internal region. However, the charge exchange rate for pickup ions in the external region is approximately 20 times smaller than the charge exchange rate in the internal region.

The model with $n_{\rm atmos} = 5 \times 10^8$ cm^{-3} (case ceie5, Table 1) corresponds to a total charge exchange rate $Q_{\rm exch} = 5.8 \times 10^{28}$ s^{-1}. The models with $n_{\rm atmos} = 10^8$ cm^{-3}, cases ceie3 and ceie4 (in Table 1) correspond to total charge exchange rates of $Q_{\rm exch} = 1.09 \times 10^{28}$ and 1.35×10^{28} s^{-1}, respectively. Finally, the models with $n_{\rm atmos} = 5 \times 10^7$ cm^{-3} (cases ceie1 and ceie2, in Table 1) correspond to charge exchange rates of $Q_{\rm exch} = 6.12 \times 10^{27}$ and 6.54×10^{27} s^{-1}, respectively.

The magnetic field profile (B_y) does not match the observational data very well for a small ionization rate, $Q_{\rm ion} = 2.1 \times 10^{27}$s^{-1} (case ceie3, Table 1), whereas the total density value in the plasma wake is much larger than observed in the case with a higher ionization rate, $Q_{\rm ion} = (3.03–4.04) \times 10^{27}$ s^{-1} (cases ceie1 and ceie2, Table 1). Hence, the models with a high charge exchange rate, $Q_{\rm exch} = (6.5–9) \times 10^{28}$ s^{-1}, are not realistic because they cannot explain the observational data.

Our analysis of all the models run (many more than presented in this paper) finds that two cases show a reasonably good fit to the observational data, better than previous MHD or electrodynamic model attempts. Surprisingly one is the unphysical model without charge exchange (case nce, Table 1, Fig. 17 (solid line)). The other is the realistic model with charge exchange, case ceie1 (Table 1), which has $n_{\rm atmos} = 5 \times 10^7$ cm^{-3} and an ionization rate $Q_{\rm ion} = 3.03 \times 10^{27}$ s^{-1}. This one is shown as the dotted lines Fig. 17. It provides global charge exchange rates $Q_{\rm p,exch} = 3.16 \times 10^{27}$ s^{-1} and $Q_{\rm c,exch} = 3.13 \times 10^{27}$ s^{-1} for plasma torus ions and pickup ions, respectively. This would correspond to an MHD model with a combined fresh ion mass-loading and the charge exchange rate, (charge exchange contributes to the momentum and energy friction terms in MHD) of 1.2×10^{28} s^{-1} (Combi et al., 2002). Therefore, we find that the interaction is dominated in roughly equal parts between primary torus ion charge exchange and secondary pickup ion charge exchange.

4. Conclusions

3D Boltzmann simulations of the interaction of the jovian plasma torus with Io, have demonstrated several new features:

- The whistler (lead front) and quasi-stationary Alfvén waves (wings) strongly affect plasma flow around Io.
- The effect of the finite ion gyroradius that results in formation of the asymmetrical boundary layer in the vicinity of Io's ionosphere is important. The plasma parameters have a strongly asymmetrical distribution across Io's wake. The kinetic behavior of ion dynamics reproduces the inverse structure of the magnetic field (due to drift current) which cannot be explained by standard MHD or electrodynamic simulations which do not account for anisotropic ion pressure. The diamagnetic effect of non-isotropic gyrating pickup ions broadens the B-field perturbation and produces increased temperatures in the flanks of the wake, as observed by the Galileo spacecraft, but not explained by previous simulations. Note that a two-fluid simulation (Saur et al., 2002) produces the double-peak signature with spatial scale much smaller than in observation.
- The cold, dense wake is produced, as in MHD, but was not produced in electromagnetic simulations without the ad hoc addition of bidirectional electrons.
- The temperatures of the electrons which are created and cooled by collision with neutrals in the exosphere and inside the ionosphere may strongly affect the pickup ion dynamics along the magnetic field and consequently the pickup distribution across the wake. In the absence of an observed global picture of the plasma distribution, the simulation serves to demonstrate the wide range of global configurations that are possible for various electron temperature descriptions. A full hybrid simulation for the plasma including an electron temperature treatment that accounts for electron–neutral collisions and a detailed neutral description would be required to produce an accurate global picture from the first principles.
- The effective conductivity of Io's ionosphere may change strongly the distribution of the magnetic field near and inside Io. The reduced conductivity (increased diffusion length, $l_{\rm d} = 0.025$) near the ionosphere and inside Io may reduce the magnetic field inside Io by 20–40% and the peak of the plasma density at the Galileo trajectory by 15%.
- The best models that fit the observational data well are: (1) the model without charge exchange and an ionization rate $Q_{\rm ion} = 4.8 \times 10^{27}$ s^{-1}, and (2) the model with ionization rate $Q_{\rm ion} = 3.03 \times 10^{27}$ s^{-1} and the total charge exchange rate $Q_{\rm exch} = 6.3 \times 10^{27}$ s^{-1}. The best MHD model had a total fresh ion mass-loading rate of 6×10^{27} s^{-1} and a charge exchange rate, which contributes to the momentum and energy friction terms, of 1.2×10^{28} s^{-1} (Combi et al., 2002). The reason for the factor of 2 difference results from the above-described pressure anisotropy effect in the kinetic simulation, and the resulting tighter plasma distribution near the equator plane defined by Io. Higher densities near the equator (i.e., at Galileo's position) result from an overall lower global ionization rate when accounting for the pressure anisotropy of pickup ions.
- For the hybrid model calculations presented here, the value of the ion gyroradius was much larger than the realistic value. This was done out of computational necessity, because using a realistic value would require many more correspondingly smaller cells and simulation particles (by factor of the cube of the ratio), which would have made a global 3D calculation impossible. In the future we plan to investigate the effects of using a realistic value with limited-domain experiments. While we expect that a smaller simulation ion gyroradius may result in a smaller asymmetry in the global simulation, we do not expect any strong changes in the plasma and magnetic field profiles because the value of the gyroradius used is still much smaller than the characteristic scale of the problem—the radius of Io. The choice of the large-than-realistic value

conserves the most important physical quantities leading to collision rates and diamagnetic effects that are quantitatively realistic. Furthermore, we do not attempt to resolve any properties smaller than the simulation gyroradius.

Acknowledgments

A.S.L. and M.R.C. were supported in part by the NASA Grant NAG5-9464 from the Applied Information Systems Research Program and NAG5-12822 from The Planetary Atmospheres Program. A.S.L. thanks the University of Michigan for hospitality during his work from April 2002 to April 2004. Computational resources were provided by the San Diego Super Computer Center (IBM Blue-Horizon), the Center for Advanced Computing University of Michigan (Parallel system IBM POWER 3 Cluster), the National Partnership for Advanced Computational Infrastructure, and the Computer Center TU of Braunschweig (Parallel Alpha-Server). The authors thanks A. Kopp and V.M. Vasyliunas for their helpful comments. A.S.L. thanks D. Markiewicz-Innes for her helpful comments.

References

Austin, J.V., Goldstein, D.B., 2000. Rarefied gas model of Io's sublimation-driven atmosphere. Icarus 148, 370–383.

Braginskii, S.L., 1965. Transport processes in a plasma. In: Leontovich, M.A. (Ed.), Reviews of Plasma Physics. Consultants Bureau, New York, pp. 205–240.

Clarke, J.T., Ajello, J., Ballester, G., Ben Jaffel, L., Connerney, J., Gèrard, J.-C., Gladstone, G.R., Grodent, D., Pryor, W., Trauger, J., Waite, J.H., 2002. Ultraviolet emissions from the magnetic footprints of Io, Ganymede and Europa on Jupiter. Nature 415, 997–1000.

Cloutier, P.A., Daniell, R.E., Dessler, A.J., Hill, T.W., 1978. A cometary ionosphere model for Io. Astrophys. Space Sci. 55, 93–112.

Combi, M.R., Kabin, K., Gombosi, T., De Zeeuw, D.L., Powell, K., 1998. Io's plasma environment during the Galileo flyby: Global three-dimensional MHD modeling with adaptive mesh refinement. J. Geophys. Res. 103, 9071–9081.

Combi, M.R., Gombosi, T.I., Kabin, K., 2002. Plasma flow past cometary and planetary satellite atmospheres. In: Mendillo, M., Nagy, A., Waite, J.H. (Eds.), Atmospheres in the Solar System: Comparative Aeronomy. Geophys. Monograph Series, vol. 130. AGU, Washington, DC, pp. 151–167.

Frank, L.A., Paterson, W.R., 1999. Intense electron beams observed at Io with the Galileo spacecraft. J. Geophys. Res. 104, 28657–28669.

Frank, L.A., Paterson, W.R., 2000. Return to Io by the Galileo spacecraft: Plasma observation. J. Geophys. Res. 105, 25363–25378.

Frank, L.A., Paterson, W.R., Ackerson, K.L., Vasyliunas, V.M., Coroniti, F.V., Bolton, S.J., 1996. Plasma observations at Io with the Galileo spacecraft. Science 274, 394–395.

Goertz, C.K., 1980. Io's interaction with the plasma torus. J. Geophys. Res. 85, 2949–2956.

Gurnett, D.A., Kurth, W.S., Roux, A., Bolton, S.J., Kennel, C.F., 1996. Galileo plasma wave observations in the Io plasma torus and near Io. Science 274, 391–392.

Ip, W.-H., 1990. Neutral gas–plasma interaction: The case of the Io plasma torus. Adv. Space Res. 10 (1), 15–18.

Kabin, K., Combi, M.R., Gombosi, T.I., DeZeeuw, D.L., Hansen, K.S., Powell, K.G., 2001. Io's magnetospheric interaction: An MHD model with day–night asymmetry. Planet. Space Sci. 49, 337–344.

Kivelson, M.G., Khurana, K.K., Walker, R.J., Warnecke, J., Russell, C.T., Linker, J.A., Southwood, D.J., Polanskey, C., 1996. Io's interaction with the plasma torus: Galileo magnetometer report. Science 274, 396–398.

Kivelson, M.G., Khurana, K.K., Russell, C.T., Joy, S.P., Volwerk, M., Walker, R.J., Zimmer, Ch., Linker, J.A., 2001. Magnetized or unmagnetized: Ambiguity persists following Galileo's encounters with Io in 1999 and 2000. J. Geophys. Res. 106, 26121–26136.

Kopp, A., 1996. Modifications of the electrodynamic interaction between Jupiter and Io due to mass loading effects. J. Geophys. Res. 101, 24943–24954.

Kopp, A., Birk, G.T., Otto, A., 1998. On the formation of Io-induced acceleration region related to jovian aurora. Planet. Space Sci. 46, 405–415.

Lellouch, E., 1996. Urey Prize Lecture. Io's atmosphere: Not yet understood. Icarus 124, 1–21.

Linker, J.A., Kivelson, M.G., Walker, R.J., 1989. The effect of mass loading on the temperature of a flowing plasma. Geophys. Res. Lett. 16 (7), 763–766.

Linker, J.A., Khurana, K.K., Kivelson, M.G., Walker, R.J., 1991. A three-dimensional MHD simulation of plasma flow past Io. J. Geophys. Res. 96, 21037–21053.

Linker, J.A., Khurana, K.K., Kivelson, M.G., Walker, R.J., 1998. MHD simulation of Io's interaction with the plasma torus. J. Geophys. Res. 103 (E9), 19867–19877.

Lipatov, A.S., 2002. The Hybrid Multiscale Simulation Technology. An Introduction with Application to Astrophysical and Laboratory Plasmas. Springer-Verlag, Berlin/Heidelberg/New York.

Lipatov, A.S., Zank, G.P., Pauls, H.L., 1998. The dynamics of an H neutral component inside the heliosphere: 2.5D particle-mesh Boltzmann simulation. J. Geophys. Res. 103, 20636–20642.

Malama, Y.G., 1991. Monte-Carlo simulation of neutral atoms trajectories in the Solar System. Astrophys. Space Sci. 176, 21–39.

Mankofsky, A., Sudan, R.N., Denavit, J., 1987. Hybrid simulation of ion beams in background plasma. J. Comput. Phys. 70, 89–116.

Marconi, M.L., Dagum, L., Smyth, W.H., 1996. Hybrid fluid/kinetic approach to planetary atmospheres: An example of an intermediate-mass body. Astrophys. J. 469, 393–401.

Neubauer, F.M., 1980. Nonlinear standing Alfvén wave current system at Io—Theory. J. Geophys. Res. 85, 1171–1178.

Ripkin, H.L., Fahr, H.J., 1983. Modification of the local interstellar gas properties in the heliospheric interface. Astron. Astrophys. 122, 181–190.

Saur, J., Neubauer, F.M., Strobel, D.F., Summers, M.E., 1999. Three-dimensional plasma simulation of Io's interaction with the Io plasma torus: Asymmetric plasma flow. J. Geophys. Res. 104, 25105–25126.

Saur, J., Neubauer, F.M., Strobel, D.F., Summers, M.E., 2002. Interpretation of Galileo's Io plasma field observations: I0, I24, and I27 flybys and close polar passes. J. Geophys. Res. 107 (SMP5), 1–18.

Saur, J., Strobel, D.F., Neubauer, F.M., Summers, M.E., 2003. The ion mass loading rate at Io. Icarus 163 (2), 456–468.

Southwood, D.J., Dunlop, M.W., 1984. Mass pickup in sub-Alfvénic plasma flow: A case study for Io. Planet. Space Sci. 32, 1079–1089.

Southwood, D.J., Kivelson, M.G., Walker, R.J., Slavin, J.A., 1980. Io and its plasma environment. J. Geophys. Res. 85, 5959–5968.

Umeda, T., Omura, Y., Matsumoto, H., 2001. An improved masking method for absorbing boundaries in electromagnetic particle simulations. Comput. Phys. Commun. 137, 286–299.

Van'yan, L.L., Lipatov, A.S., 1972. Three-dimensional hydromagnetic disturbances generated by a magnetic dipole in an anisotropic plasma. Geomagn. Aeronomy 18 (5), 316–318.

Williams, D.J., Mauk, B.H., McEntire, R.E., Roelof, E.C., Armstrong, T.P., Wilken, B., Roederer, J.G., Krimigis, S.M., Fritz, T.A., Lanzerotti, L.J., 1996. Electron beams and ion composition measured at Io and its torus. Science 274, 401–403.

Williams, D.J., Thorne, R.M., Mauk, B., 1999. Energetic electron beams and trapped electrons at Io. J. Geophys. Res. 104, 14739–14753.

Wolf-Gladrow, D.A., Neubauer, F.M., Lussem, M., 1987. Io's interaction with the plasma torus: A self-consistent model. J. Geophys. Res. 92, 9949–9961.